

A new interpretation of deformation rates in the Snake River Plain and adjacent basin and range regions based on GPS measurements

S.J. Payne,¹ R. McCaffrey,² R.W. King,³ and S.A. Kattenhorn⁴

¹*Idaho National Laboratory, P.O. Box 1625, MS 2203, Idaho Falls, ID 83415, USA. E-mail: Suzette.Payne@inl.gov*

²*Department of Geology, Portland State University, P.O. Box 751, Portland, OR 97207, USA*

³*Department of Earth, Atmospheric & Planetary Sciences, Massachusetts Institute of Technology, Cambridge, MA 02139, USA*

⁴*Department of Geological Sciences, University of Idaho, P.O. Box 443022, Moscow, ID 83844, USA*

Accepted 2012 January 6. Received 2012 January 6; in original form 2011 June 29

SUMMARY

Within the Northern Basin and Range Province, USA, we estimate horizontal velocities for 405 sites using Global Positioning System (GPS) phase data collected from 1994 to 2010. The velocities, together with geologic, volcanic, and earthquake data, reveal a slowly deforming region within the Snake River Plain in Idaho and Owyhee–Oregon Plateau in Oregon separated from the actively extending adjacent Basin and Range regions by shear. Our results show a NE-oriented extensional strain rate of $5.6 \pm 0.7 \times 10^{-9} \text{ yr}^{-1}$ in the Centennial Tectonic Belt and an ~E-oriented extensional strain rate of $3.5 \pm 0.2 \times 10^{-9} \text{ yr}^{-1}$ in the Great Basin. These extensional rates contrast with the very low strain rate within the 125 km × 650 km region of the Snake River Plain and Owyhee–Oregon Plateau, which is indistinguishable from zero ($-0.1 \pm 0.4 \times 10^{-9} \text{ yr}^{-1}$). Inversions of the velocities with dyke-opening models indicate that rapid extension by dyke intrusion in volcanic rift zones, as previously hypothesized, is not currently occurring in the Snake River Plain. This slow internal deformation, in contrast to the rapidly extending adjacent Basin and Range regions, indicates shear along the boundaries of the Snake River Plain. We estimate right-lateral shear with slip rates of 0.3–1.4 mm yr^{−1} along the northwestern boundary adjacent to the Centennial Tectonic Belt and left-lateral oblique extension with slip rates of 0.5–1.5 mm yr^{−1} along the southeastern boundary adjacent to the Intermountain Seismic Belt. The fastest lateral shearing evident in the GPS occurs near the Yellowstone Plateau where strike-slip focal mechanisms and faults with observed strike-slip components of motion are documented. The regional velocity gradients are best fit by nearby poles of rotation for the Centennial Tectonic Belt, Snake River Plain, Owyhee–Oregon Plateau, and eastern Oregon, indicating that clockwise rotation is not locally driven by Yellowstone hotspot volcanism, but instead by extension to the south across the Wasatch fault due to gravitational collapse and by shear in the Walker Lane belt resulting from Pacific–Northern America relative plate motion.

Key words: Continental tectonics: extensional; Dynamics: seismotectonics; Hotspots; Neotectonics; Kinematics of crustal and mantle deformation.

1 INTRODUCTION

The Northern Basin and Range Province in the western United States (Fig. 1) exhibits extension overprinted by hotspot volcanism that formed the prominent physiographic province of the Snake River Plain (e.g. Pierce & Morgan 1992, 2009). Previous investigators have proposed hypotheses to explain the continuing post-hotspot basalt volcanism along the track of the eastern Snake River Plain and enigmatic lack of seismicity relative to the surrounding seismically active and extending regions (e.g. Pennington *et al.* 1974; Anders & Sleep 1992; Parsons *et al.* 1998; Rodgers *et al.* 2002). Payne *et al.* (2008) conclude from an evaluation of 132 hori-

zontal Global Positioning System (GPS) velocities that the adjacent Basin and Range region in the Centennial Tectonic Belt to the northwest has an order of magnitude greater strain rate than the Snake River Plain. This result, and a similar one concluded by Chadwick *et al.* (2007) from 10 velocities, contradicts the hypothesis that Quaternary basalt dyke intrusion within Snake River Plain volcanic rift zones accommodates extension at a similar rate to that of normal faulting in the adjacent Basin and Range region (Rodgers *et al.* 1990; Parsons *et al.* 1998; Rodgers *et al.* 2002). The different, GPS-derived strain rates imply the presence of the Centennial Shear Zone (Payne *et al.* 2008), a previously unrecognized zone of right-lateral shear between the Snake River Plain and the Centennial Tectonic

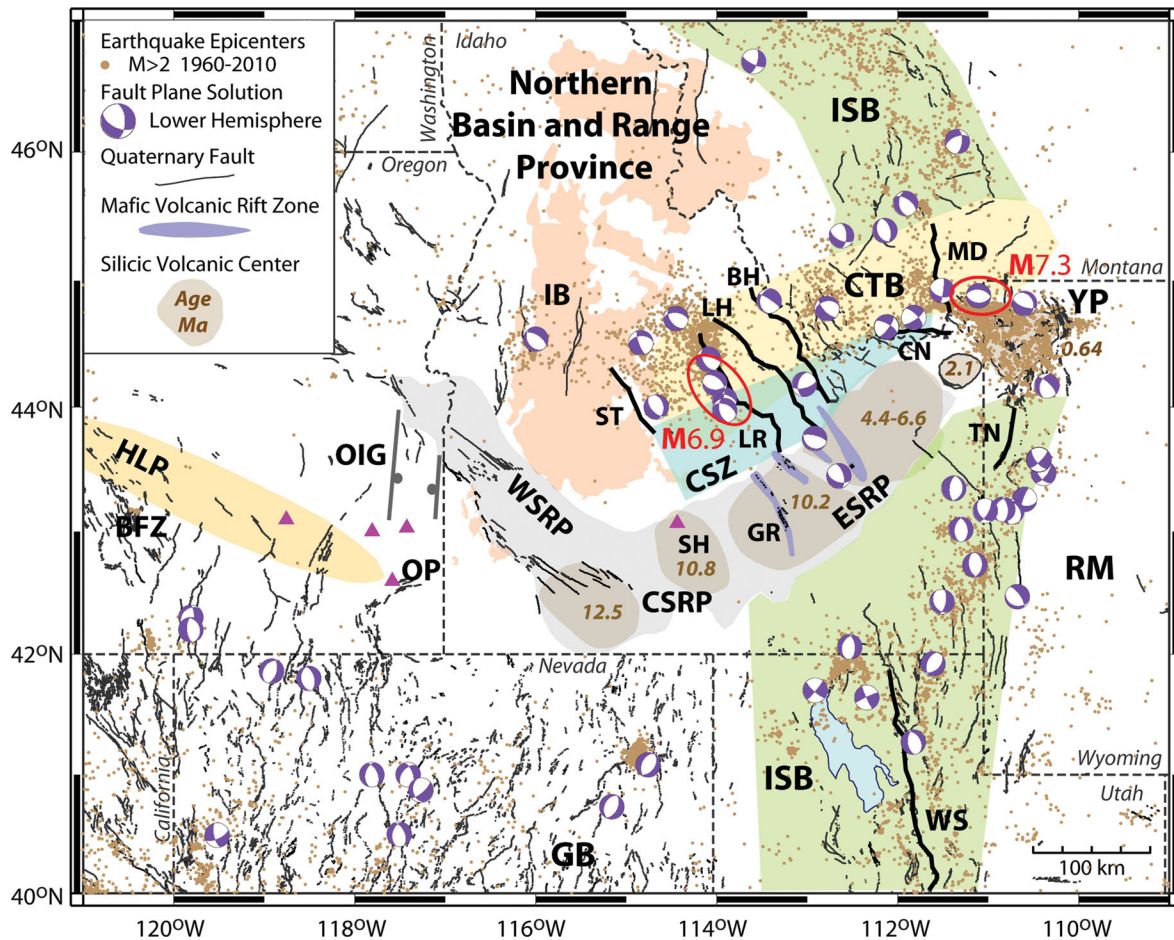


Figure 1. Map of tectonic, geologic, volcanic and seismic features of the Northern Basin and Range Province. Shaded tectonic provinces and geologic features: CTB, Centennial Tectonic Belt (Stickney & Bartholomew 1987) in yellow; CSZ, Centennial Shear Zone (Payne *et al.* 2008) in blue; HLP, High Lava Plains (Jordan *et al.* 2004) in orange; IB, Idaho Batholith (Bond *et al.* 1978; Stoeser *et al.* 2005) in salmon; ISB, Intermountain Seismic Belt (Smith & Arabasz 1991) in green; ESRP, Eastern Snake River Plain; CSR, Central Snake River Plain; and WSRP, Western Snake River Plain in grey; BFZ, Brothers Fault Zone (Walker 1969); GB, Great Basin; OIG, Oregon-Idaho Graben (Cummings *et al.* 2000); OP, Owyhee-Oregon Plateau (Shoemaker & Hart 2002); RM, Rocky Mountains; YP, Yellowstone Plateau; Quaternary faults (thin black lines) (<http://earthquake.usgs.gov/regional/qfaults/>); labels for Holocene normal faults (thick black lines) include BH, Beaverhead; CN, Centennial; LH, Lemhi; LR, Lost River; MD, Madison; ST, Sawtooth; TN, Teton, and WS, Wasatch; volcanic rift zones (blue-grey) (adapted from Kuntz *et al.* 1986, 1992) with a label for the Holocene Great Rift (GR); Holocene and Late Pleistocene volcanoes (pink triangles; Siebert & Simkin 2002) with a label for the Holocene Shoshone volcano (SH); and inferred calderas (brown shaded circular regions with age in Ma) along the NE-trending track of the Yellowstone hotspot (Pierce & Morgan 1992, 2009; Morgan & McIntosh 2005). Earthquake epicentres (brown dots) compiled for magnitudes greater than 2.0 from 1960 to 2010 (<http://www.ncedc.org/anss/catalog-search.html>). Red ellipses highlight the locations of the 1983 moment magnitude (M) 6.9 Borah Peak, Idaho and 1959 M 7.3 Hebgen Lake, Montana earthquakes. See the Supporting Information for references of lower-hemisphere focal mechanisms.

Belt (Fig. 1). Velocities also show that the Snake River Plain is included within the regional-scale clockwise rotation that extends throughout Oregon, northern Nevada and southwestern Washington (McCaffrey *et al.* 2007; Payne *et al.* 2008). Different strain rates and regional-scale clockwise rotation contradict hypotheses involving local driving forces of crustal deformation (e.g. Anders & Sleep 1992; Saltzer & Humphreys 1997; McQuarry & Rodgers 1998; Puskas & Smith 2009). The recent GPS results challenge previous hypotheses of how strain is accommodated and have implications for driving forces of crustal deformation (i.e. basal traction vs. gravity and topographic forces) in the Northern Basin and Range Province.

In this study, we present an in-depth evaluation of the 1994–2010 strengthened velocity field and expand upon the results of Payne *et al.* (2008). We update the velocity field by reoccupying selected campaign GPS sites and adding data from continuous sites and other campaigns to target regions of interest in the Snake River Plain and

adjacent Basin and Range regions. We use the new velocity field to test previous hypotheses of deformation within the Snake River Plain and to evaluate its tectonic relationship to the adjacent Basin and Range regions. We first evaluate the observed velocities in a manner similar to that in Payne *et al.* (2008). Next, we use velocities along with geologic and seismological data to design a series of block models to assess spatial variations in crustal strain rates and constrain mechanisms of deformation. We simulate rates of dyke opening within Snake River Plain volcanic rift zones to assess their significance in regional strain accommodation. We also explicitly test for post-seismic viscoelastic relaxation signals from historic moment magnitude (M) ~ 7 earthquakes. Finally, we integrate the geodetic results with geologic, volcanic and seismologic data along the track of the Yellowstone hotspot to interpret the types of deformation and possible driving forces of deformation in the Northern Basin and Range Province.

2 TECTONIC SETTING

In the past 17 Ma, the Northern Basin and Range Province has undergone extensive bimodal volcanism and crustal modifications associated with the passage of Yellowstone hotspot and Basin and Range extension (Fig. 1). Volcanic deformation in eastern Oregon and the Snake River Plain is accepted by many to have resulted from the interaction of the Yellowstone hotspot or mantle plume with the Earth's crust (e.g. Leeman 1982; Pierce & Morgan 1992, 2009; Geist & Richards 1993; Shervais & Hanan 2008; Smith *et al.* 2009). Hotspot related modification of the lithosphere is identified through an eastward progression of younger volcanic centres (Fig. 1) extending from the eastern Oregon and northern Nevada areas beginning ~17 Ma, through southern Idaho and along the eastern Snake River Plain (~16–4 Ma), and finally to the Yellowstone Plateau where caldera eruptions occurred from 2.1 to 0.64 Ma (e.g. Armstrong *et al.* 1975; Pierce & Morgan 1992, 2009; Shervais & Hanan 2008; Christiansen 2001). Recent uplift and subsidence within the Yellowstone caldera are interpreted as the result of intrusion of a sill-like magma body at mid-crustal depths (e.g. Wicks *et al.* 2006; Chang *et al.* 2007, 2010).

In eastern Oregon, extensive dyke-fed flood-basalt volcanism occurring 17–15 Ma is thought to be associated with initiation of the Yellowstone hotspot (e.g. Draper 1991; Shervais & Hanan 2008). From 16 to 10 Ma, the N-trending, topographically subdued synvolcanic Oregon–Idaho graben formed along the western margin of the North American craton shortly after eruptions of the largest volumes of flood basalts (Cummings *et al.* 2000). Isolated, dyke-fed volcanism continued into the Late Pleistocene (<60 ka) near the southern end of the Oregon–Idaho graben and in the Owyhee–Oregon Plateau (Hart *et al.* 1984; Cummings *et al.* 2000; Shoemaker & Hart 2002; Bondre 2006). Cox *et al.* (2011) attribute increased density of mid to lower-crustal depths to mafic intraplating beneath the Owyhee–Oregon Plateau.

The western Snake River Plain comprises a NW-trending graben (Fig. 1) hypothesized to have formed coeval with two different positions of the Yellowstone hotspot (Shervais *et al.* 2002; Wood & Clemmens 2002). Graben formation may have begun as early as 17 Ma in response to tumescence above the Yellowstone plume head as it raised the crust of eastern Oregon and Washington (Shervais *et al.* 2002). At 11–9 Ma, silicic and basaltic volcanism accompanied further development of the western Snake River Plain graben coeval with a later position of the Yellowstone hotspot in the central Snake River Plain (Shervais *et al.* 2002; Wood & Clemmens 2002). Basalt volcanism continued into the Mid- to Late-Pleistocene (0.2–800 ka) predominantly along the northern boundary of the western Snake River Plain (Vetter & Shervais 1992; Othberg *et al.* 1995; Shervais *et al.* 2002; Wood & Clemmens 2002). Seismic refraction, gravity and magnetic data suggest mafic densification of the crust beneath the western Snake River Plain and beyond its southern boundary into the Owyhee Plateau in Idaho (Hill & Pakiser 1967; Mabey 1976; Pakiser 1989; Mankinen *et al.* 2004).

The central and eastern Snake River Plain regions encompass silicic volcanic centres active from 12 to 4 Ma (Fig. 1) and represent the NE-trending track of the Yellowstone hotspot (e.g. Morgan & McIntosh 2005; Bonnichsen *et al.* 2008; Pierce & Morgan 1992, 2009). At each active centre, mafic crustal intrusions produced large-volume silicic eruptions that were subsequently covered by basaltic volcanism (e.g. Leeman *et al.* 2008; McCurry *et al.* 2008). Periods of increased rates of Basin and Range faulting adjacent to the Snake River Plain correlate generally with the northeast progression of younger silicic volcanic centres toward the Yellowstone

Plateau (Anders *et al.* 1989, 2009; Pierce & Morgan 1992, 2009; Anders & Sleep 1992; Rodgers *et al.* 2002; Wood & Clemmens 2002; Andrews *et al.* 2008). Following hotspot volcanism, basalt dyke intrusion continued into the Holocene (<15 ka) along NW-trending volcanic rift zones (Fig. 1) in both the central and eastern Snake River Plain regions (Kuntz *et al.* 1986, 1992). Large influxes of basaltic magma significantly modified the crust and geophysical data reveal a 10–16 km thick mafic sill at mid- to lower-crustal depths (10–30 km) beneath the central and eastern Snake River Plain regions (e.g. Sparlin *et al.* 1982; Peng & Humphreys 1998; Shervais *et al.* 2006; Stachnik *et al.* 2008; Yuan *et al.* 2010). Seismic and gravity data suggest that the mid-crustal sill may extend up to 50 km beyond the eastern Snake River Plain's physiographic boundaries into southeastern Idaho (Stachnik *et al.* 2008; DeNosaquo *et al.* 2009; Yuan *et al.* 2010).

Parts of the Basin and Range Province characterized by Quaternary normal faults, seismicity and normal faulting focal mechanisms are adjacent to the low-seismicity regions of the Snake River Plain and southern Oregon (Fig. 1). South of the Snake River Plain, the Great Basin has undergone Basin and Range extension over the last 45 Myr (Wernicke *et al.* 1987). In southern Oregon, the Basin and Range extensional province terminates along the NW-trending Brothers fault zone (Walker 1969) and the High Lava Plains Province, a Late Tertiary to Quaternary bimodal volcanic system that has a westward progression of younger ages (Jordan *et al.* 2004). East of the Snake River Plain, the Intermountain Seismic Belt is a zone of concentrated seismicity marking the eastern boundary between the actively extending Great Basin and the Rocky Mountains (e.g. Smith & Sbar 1974; Smith & Arabasz 1991; Fig. 1). The central part of the Intermountain Seismic Belt extends from the Wasatch fault to the Yellowstone Plateau and the northern zone extends north into Montana following a structural belt of Cenozoic basins bounded by Quaternary faults of diverse trends (Smith & Arabasz 1991). The Centennial Tectonic Belt broadens southeastward from the northern zone of the Intermountain Seismic Belt (Fig. 1) and is a zone of seismicity and Quaternary to Holocene normal faults adjacent to the northwestern boundary of the eastern Snake River Plain (Stickney & Bartholomew 1987). Basin and Range tectonism adjacent to the eastern Snake River Plain is thought to have initiated ~16 Ma (Rodgers *et al.* 2002). Two large, historic normal faulting earthquakes, the 1959 M 7.3 Hebgen Lake, Montana and 1983 M 6.9 Borah Peak, Idaho earthquake, occurred within the Centennial Tectonic Belt (Doser & Smith 1985; Richins *et al.* 1987). The Idaho batholith is a major Cretaceous silicic magmatic intrusion in a relatively unextended region (Gaschnig *et al.* 2009) located west of the Centennial Tectonic Belt and north of the western Snake River Plain (Fig. 1).

3 GPS OBSERVATIONS AND ANALYSES

3.1 GPS data and processing

For this study, we expand the number of GPS sites beyond those included in McCaffrey *et al.* (2007) and Payne *et al.* (2008). We include survey-mode GPS sites from the U. S. Geological Survey along five profiles (2003 Burns, Ketchum, LaGrande, Steens and Wind River), the National Geodetic Survey 1998–2000 High Accuracy Reference Network surveys, and the University of Utah (1993–2000 Snake River Plain and Yellowstone campaigns). We include data from our own new field surveys in 2008, 2009 and 2010 of 173 sites in eastern Oregon, Idaho, western Wyoming

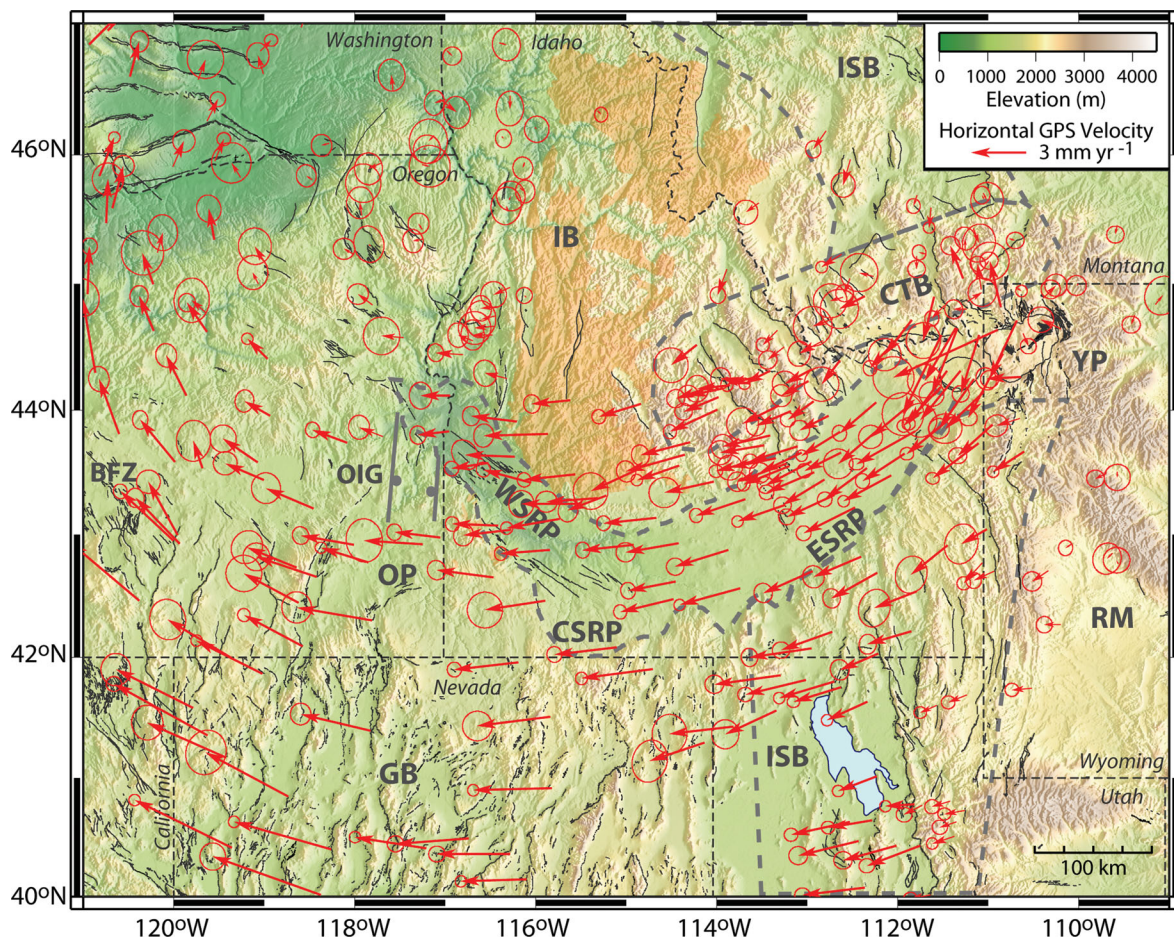


Figure 2. Shaded relief map showing observed horizontal 1994–2010 GPS velocities (red vectors) and uncertainties (at 70 per cent confidence ellipses) in the Stable North American Reference Frame (SNARF). See Fig. 1 caption for abbreviations, boundaries of tectonic provinces (dashed lines) and Quaternary fault sources. Orange shaded region shows the Idaho batholith (IB).

and southwestern Montana that includes some sites previously surveyed by the agencies mentioned. We also include phase data from seven continuous stations operated by the Idaho National Laboratory. Finally, we combined our daily position estimates and covariance matrices with those for ~200 global stations of the International GNSS Service (Dow *et al.* 2009) and between 10 (1994) and ~200 (2009) western North American stations including some from the Plate Boundary Observatory (PBO) (<http://www.earthscope.org/observatories/pbo>) and older networks, using the recent reprocessing of the Scripps Orbit and Permanent Array Center (Bock *et al.* 1997; <ftp://garner.ucsd.edu/pub/hfiles>).

We analyse the data using the GAMIT/GLOBK software (Herring *et al.* 2010) following the approach described in section 2.2 of McCaffrey *et al.* (2007). Our error model incorporates both random and correlated noise calibrated to obtain velocity uncertainties consistent with the confidence levels of their error ellipses, as described by McCaffrey *et al.* (2007). The velocities are determined relative to the Stable North American Reference Frame (SNARF; Herring *et al.* 2008) by estimating a seven-parameter transformation (three translation rates, three rotation rates and a scale rate) while minimizing the adjustments from the PBO velocity field (<http://www.earthscope.org/observatories/pbo>) of 169 continuous stations in North America.

In all of our analyses, we use only horizontal velocity estimates for which both components have one-sigma (1σ) uncertainties less

than 0.8 mm yr^{-1} . Also, we do not use the vertical velocities in our interpretation because they have large uncertainties relative to the minor vertical motions expected outside of active volcanic regions such as the Yellowstone caldera.

3.2 Regional horizontal GPS velocities

We evaluate the 405 horizontal velocities shown in Fig. 2 for the Northern Basin and Range Province (see Supporting Information). Overall, the velocity field shows regional-scale vertical-axis rotation in a clockwise sense (looking from above) that extends over the region from southwestern Montana and the Yellowstone Plateau through southern Idaho and into Oregon, similar to that described in McCaffrey *et al.* (2007) and Payne *et al.* (2008). Excluding the Yellowstone Plateau, we observe uniform magnitude velocities with southwest to westward motion within the Snake River Plain from its eastern end near Yellowstone to the western end near the Idaho–Oregon border. Velocities within the eastern Snake River Plain are faster than those in the Basin and Range regions of the Centennial Tectonic Belt to the north and Intermountain Seismic Belt to the south. On the southeastern end of the Idaho batholith and central northern Great Basin, velocities are generally similar in magnitude to those in the central part of the Snake River Plain but in western Nevada velocities exceed those in the western Snake River Plain and Owyhee–Oregon Plateau. We also observe that

velocities are slower in northeastern Oregon and western Idaho than in the southwestern part of the Idaho batholith, western Snake River Plain and Owyhee–Oregon Plateau (Fig. 2).

These observations suggest the velocity field has observable gradients arising from both rotation and strain (Fig. 3). We first estimate

the spatial variation of horizontal principal strain and vertical-axis rotation rates for the velocity field using the spherical deformation gradient tensor approach of Savage *et al.* (2001) and weighted least squares. We estimate the strain and rotation rates at 1° increments by grouping observed velocities in overlapping bins with dimensions

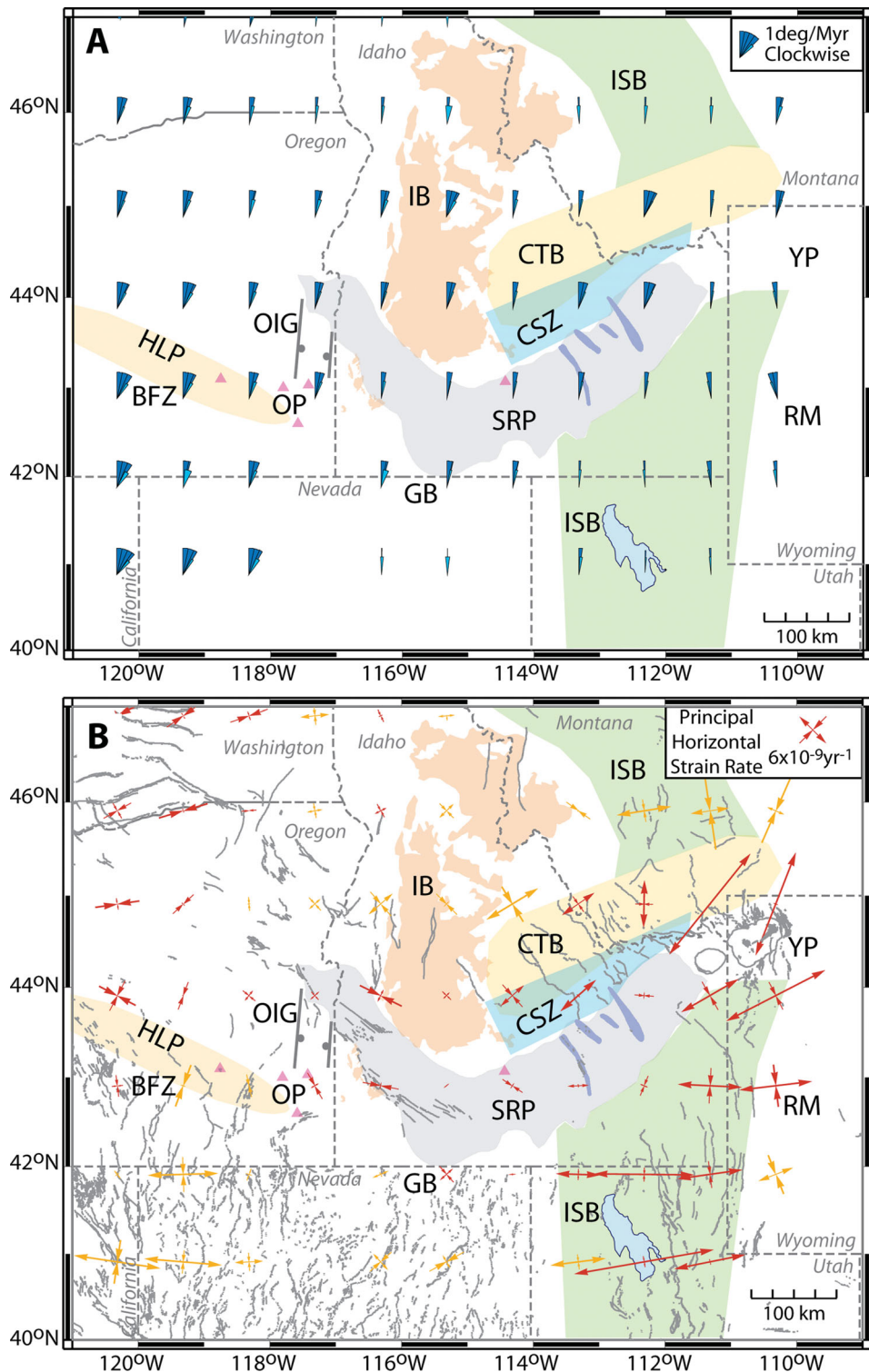


Figure 3. Rotation rates and principal horizontal strain rates at 1° increments from grouping observed velocities in overlapping bins with dimensions of 2° in longitude and 2° in latitude. (a) Velocity gradients show clockwise rotation for blue fan symbols that open from vertical to the right (dark blue) with uncertainties (pale blue). (b) Principal horizontal strain rates are shown by red arrows with uncertainties less than $2.0 \times 10^{-9} \text{ yr}^{-1}$ and orange arrows with uncertainties from $2.1 \times 10^{-9} \text{ yr}^{-1}$ to $6.0 \times 10^{-9} \text{ yr}^{-1}$. See Fig. 1 caption for abbreviations and other map contents.

of 2° in longitude and 2° in latitude. In general, the rotation rates in Fig. 3(a) are clockwise (blue fan symbols open from the vertical to the right) over the Northern Basin and Range Province and rates increase from east to west. The Centennial Tectonic Belt and Snake River Plain have smaller clockwise rotation rates than Oregon and the region along the Nevada–California border. Velocities in the Intermountain Seismic Belt along the southwestern Wyoming border reveal counter-clockwise rotation. There is very little clockwise rotation across the Wasatch fault and westward into the northern-central part of the Great Basin. Also, horizontal principal strain rates in Fig. 3(b) show extension in the Intermountain Seismic Belt and the Centennial Tectonic Belt as compared to the lower horizontal principal strain rates in the Snake River Plain and in the northern-central part of the Great Basin. The highest strain rates are located at Yellowstone, which include transient effects of recent caldera deformation (e.g. Chang *et al.* 2007, 2010; Payne *et al.* 2009).

3.3 Velocity profiles

We project the velocities onto eight profiles to expose the velocity gradients within recognized tectonic provinces of the Snake River Plain and adjacent Basin and Range regions. The first four profiles, A, B, C and D (Fig. 4), show components of the velocities that are parallel to the direction of the profiles, and therefore indicate extension for positive slopes. Two NE-oriented profiles (A and C) span the Basin and Range regions in the Centennial Tectonic Belt to the

north and the Intermountain Seismic Belt to the south of the eastern Snake River Plain. The third profile (B) is NE-oriented along the axis of the eastern Snake River Plain and includes the Yellowstone Plateau. The fourth profile (D) is E-oriented from western Oregon into the western Snake River Plain (Fig. 4).

Profiles A and C show different velocity trends than Profiles B and D (Fig. 4). In Profile A, velocities show a nearly flat slope in the western Snake River Plain and Idaho batholith (0 to 120 km) and a positive slope indicating extension across the Centennial Tectonic Belt (160–517 km; Fig. 4). We use weighted least squares, linear regressions to estimate the strain rates, given by the slopes of the velocities and their uncertainties (see Supporting Information). We estimate the strain rate of $7.3 \pm 0.4 \times 10^{-9} \text{ yr}^{-1}$ for 47 velocities across the Centennial Tectonic Belt (160 to 517 km). South of the eastern Snake River Plain, Profile C also shows a positive velocity slope across the Intermountain Seismic Belt (10–535 km) with an estimated extensional strain rate of $6.4 \pm 0.5 \times 10^{-9} \text{ yr}^{-1}$ for 20 velocities. Velocities along Profile B (80–403 km) show a nearly level slope over the eastern Snake River Plain with an estimated strain rate of $-0.4 \pm 0.6 \times 10^{-9} \text{ yr}^{-1}$ for 26 velocities, which is not differentiable from zero given the resolution of our data. At the northeastern end of the eastern Snake River Plain in Profile B, there is a steep positive slope with an estimated strain rate of $28.9 \pm 1.7 \times 10^{-9} \text{ yr}^{-1}$ associated with the Yellowstone caldera (385–536 km). The amount of scatter about the best-fitting line is much larger here than in other profile sections, suggesting that velocities are strongly modified by the well-documented transient motions near and within

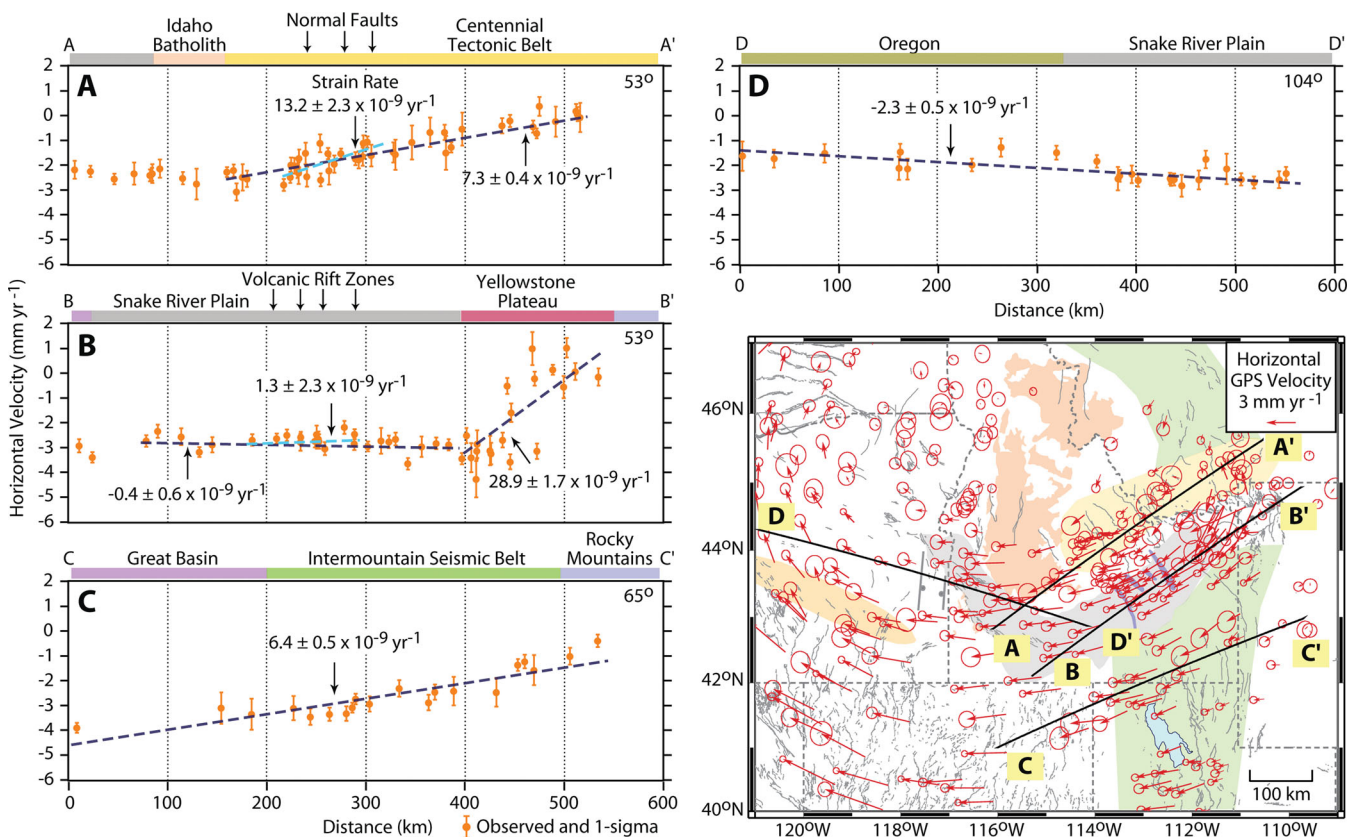


Figure 4. Profiles show components of observed horizontal velocities and one-sigma uncertainties parallel to the direction of the profiles, which indicate extension for positive slopes. Negative velocities indicate they are opposite in direction to the direction of the profile. The profile direction is indicated by letter-to-letter prime (e.g. A to A') at the azimuth shown in the upper right corner. Colour bar along the top of each profile indicates tectonic provinces. Strain rates and uncertainties (dashed black and blue lines) were calculated using weighted least-square linear regressions of velocities along the profiles (see Supporting Information). Map shows velocities and locations of profile lines; see Fig. 1 for map contents.

the Yellowstone caldera (Chang *et al.* 2007, 2010; Aly *et al.* 2009; Payne *et al.* 2009). Hence, the long-term rate of extension across the Yellowstone Plateau is not clear. Profile D shows a negative velocity slope from western Oregon across the western Snake River Plain and into the central Snake River Plain (3–552 km) indicating contraction with an estimated strain rate of $-2.3 \pm 0.5 \times 10^{-9}$ yr $^{-1}$ for 25 velocities. Contraction is also shown in Fig. 3(b) for horizontal principal strain rates near the western end of the western Snake River Plain and eastern Oregon.

The strain rates estimated for Profiles A and B in this study are similar to those estimated by Payne *et al.* (2008) but have uncertainties 2–6 times smaller as a result of using more and better velocities. Comparisons of Profiles A, B and C (Fig. 4) indicate a lower strain rate within the eastern Snake River Plain than in the adjacent Basin and Range regions. This difference is further emphasized by comparison of strain rate estimates across three Basin and Range faults and volcanic rift zones, which are previously hypothesized by some investigators to have similar rates (e.g. Parsons *et al.* 1998; Rodgers *et al.* 2002). Profile B highlights the lower strain rate of $1.3 \pm 2.3 \times 10^{-9}$ yr $^{-1}$ (187–290 km) across four Holocene to Quaternary volcanic rift zones within the eastern Snake River Plain compared to the higher strain rate of $13.2 \pm 2.3 \times 10^{-9}$ yr $^{-1}$ (218–306 km; Profile A) across three adjacent NW-trending Quaternary normal faults in the Centennial Tectonic Belt (Fig. 4). Over both long and short distances the strain rates in the Centennial Tectonic Belt are

many times higher than the strain rates in the eastern Snake River Plain.

Four profiles (E, F, G and H) show components of the velocities that are perpendicular to the direction of the profiles where negative slopes indicate either clockwise rotation or right-lateral shear or both (Fig. 5). Profiles are aligned in a southeast direction extending from the Centennial Tectonic Belt across the eastern Snake River Plain and into the Intermountain Seismic Belt (Fig. 5). The profiles all show negative velocity slopes from the Centennial Tectonic Belt into and across the eastern Snake River Plain, indicating that some velocities are consistent with a component of regional-scale clockwise rotation, right-lateral shear or both. The profiles show negative steps that are shorter wavelength than the regional clockwise rotation, indicating right-lateral shear within relatively narrow belts. By taking the difference between weighted-averaged velocities on the north side of the shear zone and the eastern Snake River Plain (see Supporting Information), we estimate slip rates of 1.8 ± 0.1 mm yr $^{-1}$, 1.4 ± 0.1 mm yr $^{-1}$, 1.1 ± 0.1 mm yr $^{-1}$ and 0.7 ± 0.2 mm yr $^{-1}$ in Fig. 5 for Profiles E, F, G and H, respectively, which we interpret as right-lateral shear along the Centennial Shear Zone (Payne *et al.* 2008). Also observed in the profiles are positive velocity slopes in the Intermountain Seismic Belt, which may indicate extension across the N-trending normal faults there (brown shaded regions in Fig. 5). Where velocities are observed between the eastern Snake River Plain and a zone of extension shown in Profiles F (410–460

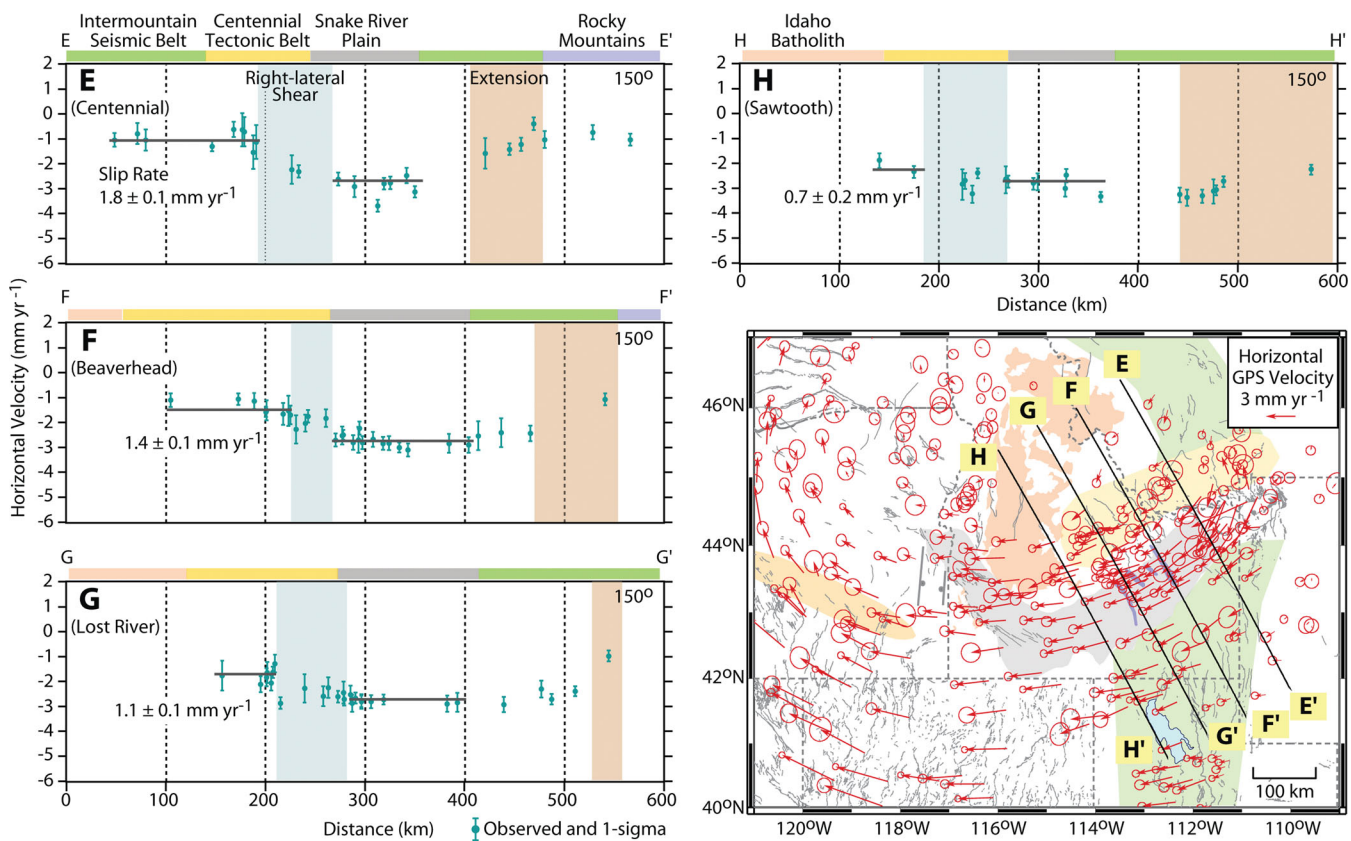


Figure 5. Profiles show components of observed horizontal velocities and one-sigma uncertainties perpendicular to the direction of the profiles, which indicate clockwise rotation or right-lateral shear or both for negative slopes. Negative velocities indicate they are opposite in direction to the direction of the profile. The profile direction is indicated by letter-to-letter prime (e.g. E to E') at the azimuth shown in the upper right corner. Colour bar along the top of each profile shows tectonic provinces. Solid grey lines emphasize velocity steps and show the velocities along the profiles used to estimate slip rates for right-lateral shear. Slip rates were estimated by taking the difference of the weighted average velocities between velocities northwest of the right-lateral shear zone (blue shading) and the weighted average velocity for Snake River Plain (see Supporting Information). Brown shading indicates regions where profile lines are oblique to N-trending normal faults and associated extension. Map shows velocities and locations of profile lines; see Fig. 1 for map contents.

km) and G (410–530 km), there is a slight positive increase, indicating some left-lateral shear between the eastern Snake River Plain and the Intermountain Seismic Belt.

Overall, profiles in Fig. 5 indicate a NE-trending zone of right-lateral shear in the Centennial Shear Zone with slip rates that are lower in the southwest ($0.7 \pm 0.2 \text{ mm yr}^{-1}$ and $1.1 \pm 0.1 \text{ mm yr}^{-1}$) and increase to the northeast ($1.4 \pm 0.1 \text{ mm yr}^{-1}$ and $1.8 \pm 0.1 \text{ mm yr}^{-1}$). Fig. 2 shows that velocities are generally similar in magnitude between the eastern Snake River Plain and Centennial Tectonic Belt southwest of the Sawtooth fault (Profile H; Fig. 5) whereas velocities in the eastern Snake River Plain are faster than those in the Centennial Tectonic Belt near the Centennial fault (Profile E; Fig. 5).

4 KINEMATIC INTERPRETATIONS

We apply a microplate, or block model, approach to describe the pattern of deformation within the Northern Basin and Range Province. The velocity profiles suggest that the upper crust in this region is deforming in a discontinuous manner, indicated by different strain rates along the profiles in Fig. 4 between the Snake River Plain and adjacent Basin and Range regions (Centennial Tectonic Belt and Intermountain Seismic Belt). In addition, Fig. 2 shows regional-scale clockwise rotation over the Northern Basin and Range Province and Fig. 3(b) shows large regions with little deformation (e.g. Snake River Plain and eastern Oregon and Washington). We employ the block-model approach because it allows us to interrogate the velocity field using either discrete boundaries or continuous deformation. That is, we can test the significance of boundaries between these tectonic provinces, assess slip rates along their boundaries, and estimate long-term deformation (i.e. permanent deformation) within these provinces.

To guide our kinematic interpretations of the velocity field, we use the block-model inverse approach in TDEFNODE (McCaffrey 2009), an update of the program DEFNODE (McCaffrey 1995, 2002). We use TDEFNODE to invert velocities, earthquake slip vectors, and dyke-opening rates to solve simultaneously for the angular velocities of blocks and uniform horizontal strain rate tensors within selected blocks. The analyses account for the rotational velocities and anelastic strain rates in elastic–plastic crustal blocks. The best-fit set of parameters is found by simulated annealing (Press *et al.* 1989) that minimizes the reduced chi-squared (χ^2_η) of the misfit to the weighted data. Parameter uncertainties are estimated by a linear approximation that is used to build the parameter covariance matrix.

4.1 Northern basin and range regional block model

We develop a block model of the Northern Basin and Range Province to test a range of possibilities for deformation in the Snake River Plain and adjacent Basin and Range regions. Block boundaries separate tectonic provinces based on knowledge of geology, seismicity, volcanism, active tectonic faults and regions with observed differences in surface velocities. We compile slip vectors from focal mechanisms (see Supporting Information) of earthquakes located near block boundaries. We also estimate dyke-opening rates to constrain horizontal motion along block boundaries that represent volcanic rift zones. Fig. 6 shows the block model configuration for the Northern Basin and Range with the tectonic provinces, geologic and seismologic data. Here, we give a general discussion of the blocks and their boundaries; further details are included in the Supporting Information.

We constructed a block model for the Snake River Plain to test the location and kinematics of its boundaries and whether or not volcanic rift zones contribute to its internal deformation. The block perimeter of the Snake River Plain in some places follows and in other places deviates from its physiographic boundaries. For example, the northwestern and southeastern boundaries of the ESRP block extend beyond the physiographic boundaries to include velocities more similar in magnitude to those in the Snake River Plain than those in the adjacent Centennial Tectonic Belt block (called CTBt) and Idaho–Wyoming border block (called IdWy), respectively (Fig. 6b). We separate the Snake River Plain into three blocks along two volcanic rift zones: (1) the eastern Snake River Plain block (ESRP) is separated from the central Snake River Plain block (CSRP) along the Great Rift, an 85-km long Holocene volcanic rift zone with eight mafic dyke-fed episodes occurring 2–15 ka (Kuntz *et al.* 1986, 2002, 2007) and (2) the western Snake River Plain block (WSRP) is separated from CCSR block near source vents of the Shoshone volcanic field that has Quaternary basalt flows as young as $\sim 10\,000$ yr (Kuntz *et al.* 1986). Although not part of the Snake River Plain, the Owyhee–Oregon Plateau block (Owhy) has velocities more similar to those in the WSRP block than those to the south in the western Basin and Range block (WBnR). The Owhy block shares its eastern boundary with the WSRP block (Fig. 6b).

Outside of the Snake River Plain, we separate recognized tectonic provinces and assess the significance of these boundaries (Fig. 6). North of the Snake River Plain, we create three blocks associated with the Centennial Tectonic Belt and northern part of the Intermountain Seismic Belt (Fig. 6) based largely on differences in the velocities: (1) CTBt block, (2) SwMT block (southwest Montana) and (3) EMnt block (eastern Montana, which refers to the easternmost extent of Basin and Range faults). Farther west, we separate the CTBt block from the Idaho batholith block (IBat). Because we lack velocities northwest of the IBat and SwMT blocks, we create the eastern Washington block (EWas), a large block similar to that used by McCaffrey *et al.* (2007). To the west and south of the Snake River Plain, we include a block for eastern Oregon (called EOre) and two blocks for the Great Basin, one called GrBn and the other WBnR based on McCaffrey (2005) (Fig. 6). Although we show the westernmost blocks (OrBR, YFTB and Wena) from McCaffrey *et al.* (2007) in Fig. 6(b), we did not include these blocks in the inversions. Velocities in these three blocks are affected by elastic strain of the Cascadia subduction zone (McCaffrey *et al.* 2007), which we do not include in this study. We also exclude velocities west of -119°W longitude in the EOre block for this same reason. Finally, east of the Snake River Plain and Great Basin, we set up the IdWy block and the North America block (NoAm). The NoAm block is used to establish a reference frame for the other blocks, and is fixed relative to SNARF. Throughout, we use North America as the indicator of SNARF.

4.2 Inversion results

4.2.1 Preferred model

From a series of block models, we determine the preferred model, which we then use to evaluate the significance of dyke-opening rates, slip rates along block faults, strain rates in tectonic provinces and the significance of post-seismic viscoelastic relaxation effects. To arrive at a preferred model, we start with a model in which all blocks rotate with the same angular velocity relative to North America. We then add boundaries and determine their statistical significance in separating tectonic provinces. This approach allows

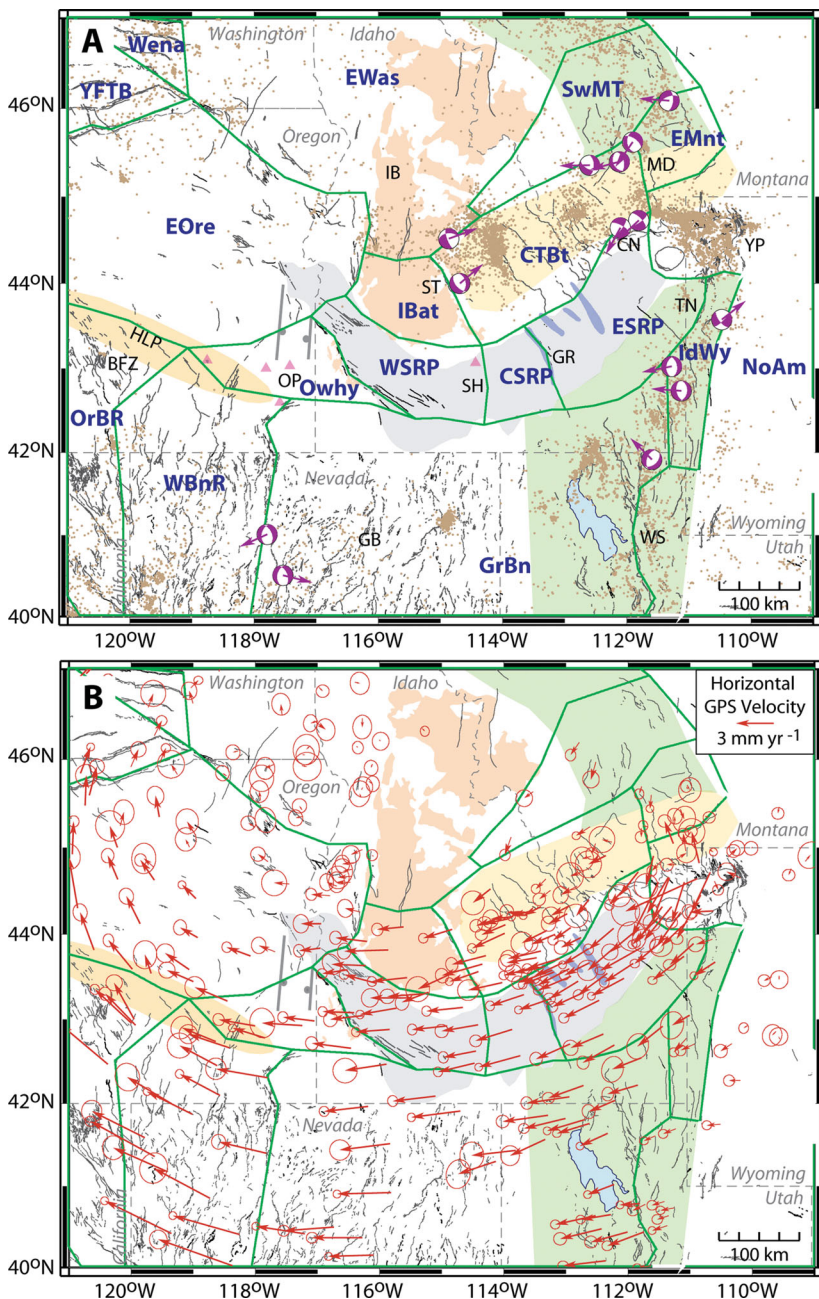


Figure 6. Maps showing the block model (green lines) with block names (blue letters) for the Northern Basin and Range Province superimposed on: (a) tectonic provinces (shaded regions as presented in Fig. 1), Quaternary faults (thin black lines), volcanic rift zones (blue-grey), Holocene and Late Pleistocene volcanoes (pink triangles), lower-hemisphere focal mechanisms with slip vectors (purple and white circles and purple arrows) (see Supporting Information), and earthquake epicentres for magnitudes greater than 2.0 from 1960 to 2010 (brown dots); and (b) observed horizontal velocities (red vectors) with 70 per cent confidence ellipses in the Stable North American Reference Frame. See Fig. 1 caption for other map contents.

us to assess by fit to the observations whether any increase in model complexity due to the addition of more boundaries or strain rate tensors is statistically warranted. We determine the preferred model by dividing blocks until changes in fit are not significant. We calculated the statistical significance using the χ^2 and degrees of freedom in F-distribution tests between two models. We apply the maximum confidence level of ≥ 99 per cent to indicate one model with added boundaries has a better fit to the data over a second model (Stein & Gordon 1984).

In total, we test 14 models (Table 1) in the inversions with geodetic and earthquake data to determine ctb9 as the preferred model (see Supporting Information for all model results). Model nb11

with all of the blocks combined together and rotating about the same angular velocity has the highest $\chi^2_\eta = 5.01$ (Table 1) and indicates that vertical-axis rotation alone does not fit the data. As we separate blocks and add a strain rate tensor in the GrBn block (Fig. 7a), we observe decreases in χ^2_η that show model nbr3 ($\chi^2_\eta = 1.72$) has a better fit to the data at the ≥ 98 per cent confidence level than models nb13 ($\chi^2_\eta = 3.36$) and nb16 ($\chi^2_\eta = 2.08$; Tables 1 and 2). Comparison of these three models indicate better fits to the data with separate poles of rotation for the EWAs, EOre, IdWy, and GrBn blocks and combined block regions of CTBt/SwMT/EMnt/IBat and ESRP/CSRP/WSRP/Owhy. When we include a strain rate tensor in the combined block region of

Table 1. Model and velocity misfits from the inversions.

Model name	Model fit		Fit of GPS velocities within a single block or multiple blocks with the same pole of rotation (χ^2_η , Name of blocks)			
	χ^2_η	NP	DOF			
nb11	5.01	3	537	5.01, EWas/EOr/EBnR/GrBn/IdWyr/ESRP/CSRP/WSRP/Owhy/CTBt/SwMT/EMnt/IBat	4.44, GrBn/WBnR/IdWyr ^a	
nb13	3.36	9	532	2.89, EWas/EOr/ESRP/CSRP/WSRP/Owhy/CTBt/SwMT/EMnt/IBat	1.65, GrBn ^a	1.60, WBnR
nb16	2.08	18	529	2.71, EOr/ESRP/CSRP/WSRP/Owhy/CTBt/SwMT/EMnt/IBat	1.65, GrBn ^a	1.25, IdWyr
nbr3	1.72	24	525	3.97, CTBt/SwMT/EMnt/IBat	1.65, GrBn ^a	1.24, IdWyr
ctb9	1.21	27	522	1.54, CTBt/SwMT/EMnt/IBat ^a	0.71, ESRP/CSRP/WSRP/Owhy	1.60, WBnR
esa9	1.21	52	497	1.46, CTBt/SwMT/EMnt/IBat ^a	0.71, ESRP/CSRP/WSRP/Owhy	1.24, IdWyr
ctb7	1.16	30	520	1.34, CTBt/SwMT/EMnt ^a	0.71, ESRP/CSRP/WSRP/Owhy	1.49, IdWyr
wsr1	1.21	30	519	1.54, CTBt/SwMT/EMnt/IBat ^a	0.78, CSRP/WSRP/Owhy	1.66, WBnR
max1 ^b	1.23	27	522	1.54, CTBt/SwMT/EMnt/IBat ^a	0.93, CSRP/WSRP/Owhy	1.65, GrBn ^a
vrz1 ^b	1.49	27	522	1.54, CTBt/SwMT/EMnt/IBat ^a	2.48, CSRP/WSRP/Owhy	0.60, EOr
wsr2	1.21	30	519	1.54, CTBt/SwMT/EMnt/IBat ^a	0.79, WSRP/Owhy	0.66, ESRP/CSRP
max2 ^b	1.23	27	522	1.54, CTBt/SwMT/EMnt/IBat ^a	1.10, WSRP/Owhy	0.57, EOr
wsr3	1.21	33	516	1.54, CTBt/SwMT/EMnt/IBat ^a	0.79, WSRP/Owhy	0.68 ESRP
max3 ^b	1.29	27	522	1.54, CTBt/SwMT/EMnt/IBat ^a	1.61, WSRP/Owhy	1.00 CSR
					0.07 CSR	0.57, EOr
					1.02 ESRP	1.59, WBnR
					0.57, EOr	1.24, IdWyr

χ^2_η , Reduced chi-square; NP, Number of Free Parameters; DOF, degrees of freedom.

^aBlock has a strain rate tensor.

^bModel includes dyke-opening rates.

CTBt/SwMT/EMnt/IBat, the χ^2_η decreases to 1.21 for model ctb9 (Fig. 7b) resulting in a better fit to the data at the ≥ 99 per cent confidence level as compared to model nbr3 (Table 2). There is a modest decrease in χ^2_η to 1.16 when we include a boundary representing the Sawtooth fault (Fig. 1) to separate the IBat block from combined block region of CTBt/SwMT/EMnt (Table 1), which is significant only at the 69 per cent confidence level (Table 2). Comparison of models ctb9 and ctb7 indicates no significant improvement (69 per cent < 99 per cent) is found by separating the Centennial Tectonic Belt into smaller blocks. We also observe a similar result when the Snake River Plain and Owyhee–Oregon Plateau are separated into smaller blocks by boundaries representing the volcanic rift zones: Great Rift in model wsr1, Shoshone in model wsr2 and both Great Rift and Shoshone in model wsr3 (Figs 8a–c, respectively). Models wsr1, wsr2 and wsr3 all have $\chi^2_\eta = 1.21$ (Table 1), similar χ^2_η to model ctb9 resulting in improved fits to the data only at the 50–53 per cent confidence levels (Table 2). From these comparisons, we conclude that including volcanic rift zones within the Snake River Plain does not significantly improve the fits to the velocities (Figs 8a–c). Finally, we ran model esa9 using the same block model as ctb9 but allowing elastic strain accumulation along block boundaries, which resulted in a $\chi^2_\eta = 1.21$ similar to ctb9 (Table 1). Including elastic strain accumulation predicts observable but small velocities ($< 1 \text{ mm yr}^{-1}$) only at GPS sites near the N-trending boundaries of the GrBn block and along the boundary between Yellowstone Plateau and EMnt block. Hence, model esa9 indicates there is very little resolvable elastic strain accumulation on faults near the Snake River Plain. We cannot resolve fault-locking depths since tests with a suite of locking-depths indicate the data are not sensitive to fault locking (see Supporting Information). From comparisons of these model results, we designate ctb9 as our preferred model to further evaluate deformation in the Northern Basin and Range Province.

4.2.2 Test of dyke-opening rates

A recent hypothesis suggests that extension via dyke-intrusion in the Snake River Plain keeps pace with extension by normal faulting in the adjacent Basin and Range provinces (Rodgers *et al.* 1990; Parsons *et al.* 1998; Rodgers *et al.* 2002). To explicitly test this hypothesis, we estimate extension rates, or what we refer to as dyke-opening rates, using two methods and evaluate whether or not models that satisfy these rates along the Great Rift and Shoshone volcanic rift zones fit the velocities (Fig. 8). First, estimates of dyke-opening rates are derived from volcanic, rift-perpendicular extension inferred by Holmes *et al.* (2008) at three locations within the Great Rift volcanic rift zone. Using their estimated eruptive time periods and extension estimates, we calculate horizontal dyke-opening rates that range from 0.16 to 2.03 mm yr^{-1} (see Supporting Information). Secondly, we estimate the range of dyke-opening rates to be 0.96 to 1.36 mm yr^{-1} from the GPS-derived extension rate across three NW-trending normal faults in the Centennial Tectonic Belt ($13.2 \pm 2.3 \times 10^{-9} \text{ yr}^{-1}$ over 88 km for Profile A in Fig. 4).

For comparisons of inversion results, models max1, max2, max3 and vrz1 are identical to models wsr1, wsr2, wsr3 and wsr1 respectively, except in the former we constrain the volcanic rift zones to have dyke-opening rates and directions within the ranges listed in Table 3. Models max1, max2 and max3 result in predicted horizontal dyke-opening rates of 0.16–0.33 mm yr^{-1} (Figs 8c, d and f). These three models all have degraded fits to the velocities (higher $\chi^2_\eta = 1.23$ –1.29; Table 1) at the 60–81 per cent confidence level (Table 2)

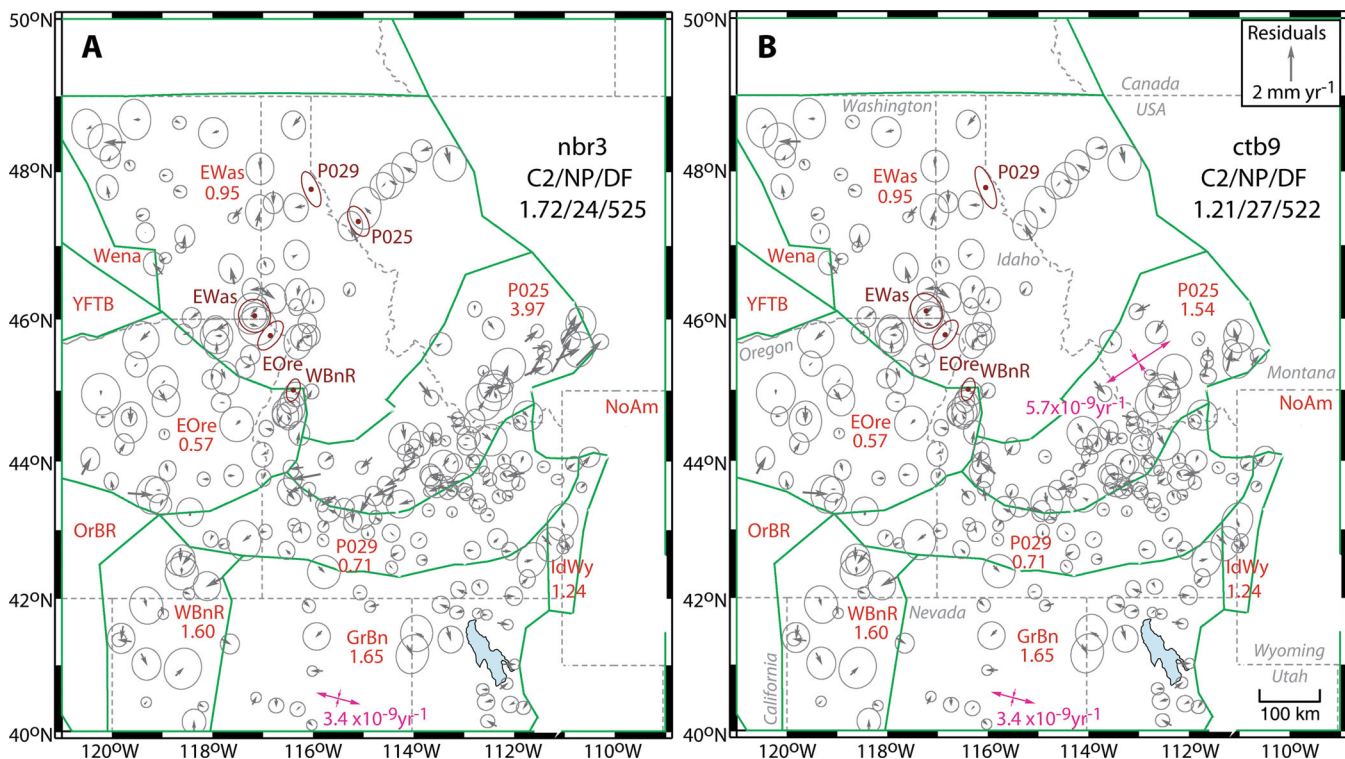


Figure 7. Maps showing inversion results with residual velocities (grey vectors with 70 per cent confidence ellipses) for models: (a) nbr3 and (b) ctb9. These results show the significance of including strain rates in the Centennial Tectonic Belt blocks (labelled P025) and Great Basin block (GrBn) when separating these tectonic provinces from the blocks for the Snake River Plain and Owyhee–Oregon Plateau (labelled P029), Western Basin and Range (WBNR), Idaho–Wyoming border (IdWY), and Eastern Washington (EWAs). The model name is given above the inversion results shown below C2/NP/DF, which corresponds to reduced chi-square (C2), number of free parameters (NP) and degrees of freedom (DF). Each block (green lines) is labelled with its name (red letters) and reduced chi-square (red number) fit of the velocities. Brown dots with 70 per cent confidence ellipses show locations of the poles of rotation. Poles (brown letters) are labelled for individual block names or pole numbers for block combinations (P029, ESRP/WSRP/CSRP/Owhy and P025, CTBt/SwMT/EMnt/IBat). Principal horizontal strain rates (pink arrows) are labelled with the extensional strain rate (pink letters).

when compared to models wsr1, wsr2 and wsr3 (all lower with $\chi^2_\eta = 1.21$; Table 1) that did not impose extension along the Great Rift and Shoshone volcanic rift zones. In fact, model wsr2 fits the velocities better with a very small component of oblique convergence (0.1 mm yr^{-1}) (Fig. 8b) instead of extension along the Shoshone volcanic rift zone (Fig. 8e). When both the Great Rift and Shoshone volcanic rift zones are included, model wsr3 with extension across the Great Rift ($<0.3 \text{ mm yr}^{-1}$) and oblique convergence across Shoshone ($<0.4 \text{ mm yr}^{-1}$; Fig. 8c) fit the velocities better than model max3, which has extension across both volcanic rift zones (Fig. 8f). Compared with model wsr1 ($\chi^2_\eta = 1.21$), we observe an even greater degraded fit at the 99 per cent confidence level (Table 2) for model vrz1 ($\chi^2_\eta = 1.49$) where we apply a dyke-opening rate to be the same as the GPS-derived normal-faulting extension rate. Results of these four inversions contradict the hypothesis that extension by means of dyke-intrusion in the Snake River Plain presently keeps pace with normal-faulting extension in the adjacent Basin and Range provinces. We conclude that at present, dyke-intrusion in Snake River Plain volcanic rift zones does not play a significant role in accommodating extension.

4.2.3 Block boundary kinematics

We explore the kinematics of the boundaries between the Snake River Plain and adjacent regions using the preferred model ctb9. The largest-predicted slip rates are along boundaries at the eastern end of the Snake River Plain and Owyhee–Oregon Plateau block

(ESRP/CSRP/WSRP/Owhy) between it and the IdWY block and combined block region of CTBt/SwMT/EMnt/IBat. We observe right-lateral strike-slip motion along the northwestern boundary of the ESRP/CSRP/WSRP/Owhy block that decreases southwestward from 1.4 mm yr^{-1} near Yellowstone to $<0.3 \text{ mm yr}^{-1}$ southeast of the Sawtooth fault (Fig. 9). Slip rates with left-lateral oblique extension at $1.3\text{--}1.5 \text{ mm yr}^{-1}$ are shown along the southeastern boundary between the ESRP/CSRP/WSRP/Owhy and IdWY blocks. The shear and oblique extension seen in the predicted slip rates (Fig. 9) are consistent with the velocity steps in Profiles E, F and G (Fig. 5). The largest slip rates, closest to the Yellowstone Plateau, are near earthquake focal mechanisms showing right-lateral strike-slip motion along the northwestern boundary and left-lateral strike-slip motion along the southeastern boundary of the ESRP/CSRP/WSRP/Owhy block (Fig. 9).

In the central part of the Snake River Plain, slip rates have magnitudes of $\leq 0.5 \text{ mm yr}^{-1}$ along both the northern and southern boundaries of the ESRP/CSRP/WSRP/Owhy block (Fig. 9). At these locations the magnitudes of velocities in the Centennial Tectonic Belt, Snake River Plain and Great Basin are similar; thus, there is very little slip across the boundaries. Farther west along the southern boundary of the ESRP/CSRP/WSRP/Owhy block we observe right-lateral oblique normal slip between it and the GrBn block and convergence between it and the WBNR block ($\leq 1.0 \text{ mm yr}^{-1}$ in Fig. 9). Velocities in the GrBn and WBNR blocks are generally faster to the west than those in the western Snake River Plain and the Owyhee–Oregon Plateau (Fig. 2). Right-lateral shear would

Table 2. Results of F distribution tests for model pairs.

Model	χ^2_η	DOF	p (per cent)
nb13	3.36	532	100
nb11	5.01	537	
nb16	2.08	529	100
nb13	3.36	532	
nbr3	1.72	532	98
nb16	2.08	529	
ctb9	1.21	522	100
nbr3	1.72	532	
ctb7	1.16	520	69
ctb9	1.21	522	
wsr1	1.21	519	50
ctb9	1.21	522	
wsr2	1.21	519	51
ctb9	1.21	522	
wsr3	1.21	516	53
ctb9	1.21	522	
wsr1	1.21	519	60
max1	1.23	522	
wsr2	1.21	519	62
max2	1.23	522	
wsr3	1.21	516	81
max3	1.29	522	
wsr1	1.21	519	99
vrz1	1.49	522	

χ^2_η , Reduced chi-square; DOF, degrees of freedom; p, Probability that misfit variances are from different distributions.

be expected because the magnitudes of the velocities in the WBnR block across southern Oregon exceed those in the western Snake River Plain and the Owyhee–Oregon Plateau (Fig. 2). For example, shear could be accommodated by right-lateral strike-slip motions along the Brothers fault zone, which is located near the western end of the Owyhee block (Fig. 6a) and thought to be the northern boundary of Basin and Range extension across southern Oregon (Lawrence 1976).

Along the northern boundary of the ESRP/CSRP/WSRP/Owyhee block (south of the IBat block), slip-rate vectors have convergent motions ($\leq 0.9 \text{ mm yr}^{-1}$) (Fig. 9). The velocities in the IBat block can be fit with an angular velocity equal to that for the combined block region of CTBt/SwMT/EMnt (models ctb9 and ctb7; Table 1). We lack sufficient velocities to separately calculate a strain rate in the IBat block, but magnitudes of six velocities across this block suggest extension is not similar to that in the adjacent Centennial Tectonic Belt. The small differences in magnitudes of velocities in the Idaho batholith and western Snake River Plain suggest that the Idaho batholith is moving west with the Snake River Plain and slip along this boundary may not be significant (Fig. 2).

Along the western boundaries of the ESRP/CSRP/WSRP/Owyhee and CTBt/SwMT/EMnt/IBat blocks adjacent to the EOre block, slip rates show convergence ($\leq 1.3 \text{ mm yr}^{-1}$; Fig. 9) consistent with a westward decrease in magnitudes (Fig. 2). Contraction along the boundary between the IBat and EOre blocks coincides with a nearly vertical lithospheric suture proposed by Leeman *et al.* (1992, 2009) along the western edge of the Idaho batholith. While we choose to model a discrete boundary between the ESRP/CSRP/WSRP/Owyhee and EOre blocks, contraction may be distributed over a larger region (Fig. 4d). To the north between the EWAs and EOre blocks, we observe normal slip (Fig. 9), which is consistent with Quaternary

normal faults mapped along the west side of the Idaho batholith (Fig. 1). We lack velocities in the northern part of the Idaho batholith to determine the nature of deformation along the western boundary of the Idaho batholith.

Outside of the Snake River Plain and Owyhee–Oregon Plateau we show modeled slip-rate vectors for three boundaries. Along the northern boundary between the CTBt/SwMT/EMnt/IBat and EWAs blocks, Fig. 9 shows right-lateral oblique convergent motions increasing southwestward from 0.4 to 1.3 mm yr^{-1} . The nature and location of this boundary are not well constrained since there are few velocities near the boundary between these two blocks (Fig. 6b). To the south of the Snake River Plain and Owyhee–Oregon Plateau, the two N-oriented boundaries of the GrBn block show extensional slip rates (1.1 – 1.5 mm yr^{-1}) except along the northern part closest to the Owyhee–Oregon Plateau between the WBnR and GrBn blocks, which shows oblique convergence (Fig. 9). Extension along GrBn block boundaries is consistent with other studies for the Great Basin (e.g. Hammond & Thatcher 2004; Hammond *et al.* 2011).

4.2.4 Strain and rotation rates

We estimate horizontal strain rate tensors and vertical-axis rotation rates using observed velocities in four regions defined from the preferred model ctb9: (1) Centennial Tectonic Belt; (2) Great Basin; (3) Snake River Plain and Owyhee–Oregon Plateau and (4) eastern Oregon. After subtracting out their respective components of rotation, we observe recognizable gradients in residual velocities north and south of the Snake River Plain, which are not observed in the Snake River Plain, Owyhee–Oregon Plateau and eastern Oregon (Fig. 10). From observed velocities, we estimate horizontal extensional strain rates of $5.6 \pm 0.7 \times 10^{-9} \text{ yr}^{-1}$ oriented $N57^\circ\text{E}$ for the Centennial Tectonic Belt and $3.5 \pm 0.2 \times 10^{-9} \text{ yr}^{-1}$ oriented $N104^\circ\text{E}$ for the Great Basin (similar to the extensional strain rate of Hammond *et al.* 2011 for the Great Basin). In contrast, we estimate strain rates of $-0.1 \pm 0.4 \times 10^{-9} \text{ yr}^{-1}$ oriented $N72^\circ\text{E}$ for the Snake River Plain and Owyhee–Oregon Plateau and $-1.1 \pm 0.7 \times 10^{-9} \text{ yr}^{-1}$ oriented $N110^\circ\text{E}$ for eastern Oregon (Fig. 10). We consider these strain rates indistinguishable from zero. These estimates indicate higher extensional rates north and south of the Snake River Plain and a much lower rate of deformation within the Snake River Plain, Owyhee–Oregon Plateau and eastern Oregon.

The vertical-axis rotations are all clockwise but at different rates in the four regions. Eastern Oregon has the highest clockwise rotation rate of $-0.42 \pm 0.04^\circ \text{ Myr}^{-1}$ (similar to $-0.41 \pm 0.02 \text{ Myr}^{-1}$ of McCaffrey *et al.* 2007) whereas the Great Basin has the lowest rate at $-0.09 \pm 0.01^\circ \text{ Myr}^{-1}$. The Snake River Plain and Owyhee–Oregon Plateau region has a rotation rate of $-0.30 \pm 0.03^\circ \text{ Myr}^{-1}$ and is greater than the rate of $-0.23 \pm 0.03^\circ \text{ Myr}^{-1}$ for the Centennial Tectonic Belt and that for the Great Basin. The greater rotation rate in the Snake River Plain over the Centennial Tectonic Belt indicates relative motion along the boundary or else the two regions would have the same rotation rate.

4.2.5 Effects of post-seismic viscoelastic relaxation

Some workers postulate that the velocity field for the Snake River Plain and adjacent Basin and Range regions may contain signals generated by mantle relaxation following large historical earthquakes in the region (Nishimura & Thatcher 2003; Puskas *et al.* 2007). Puskas *et al.* (2007) and Puskas & Smith (2009) corrected their velocities for such relaxation signals based on theoretical

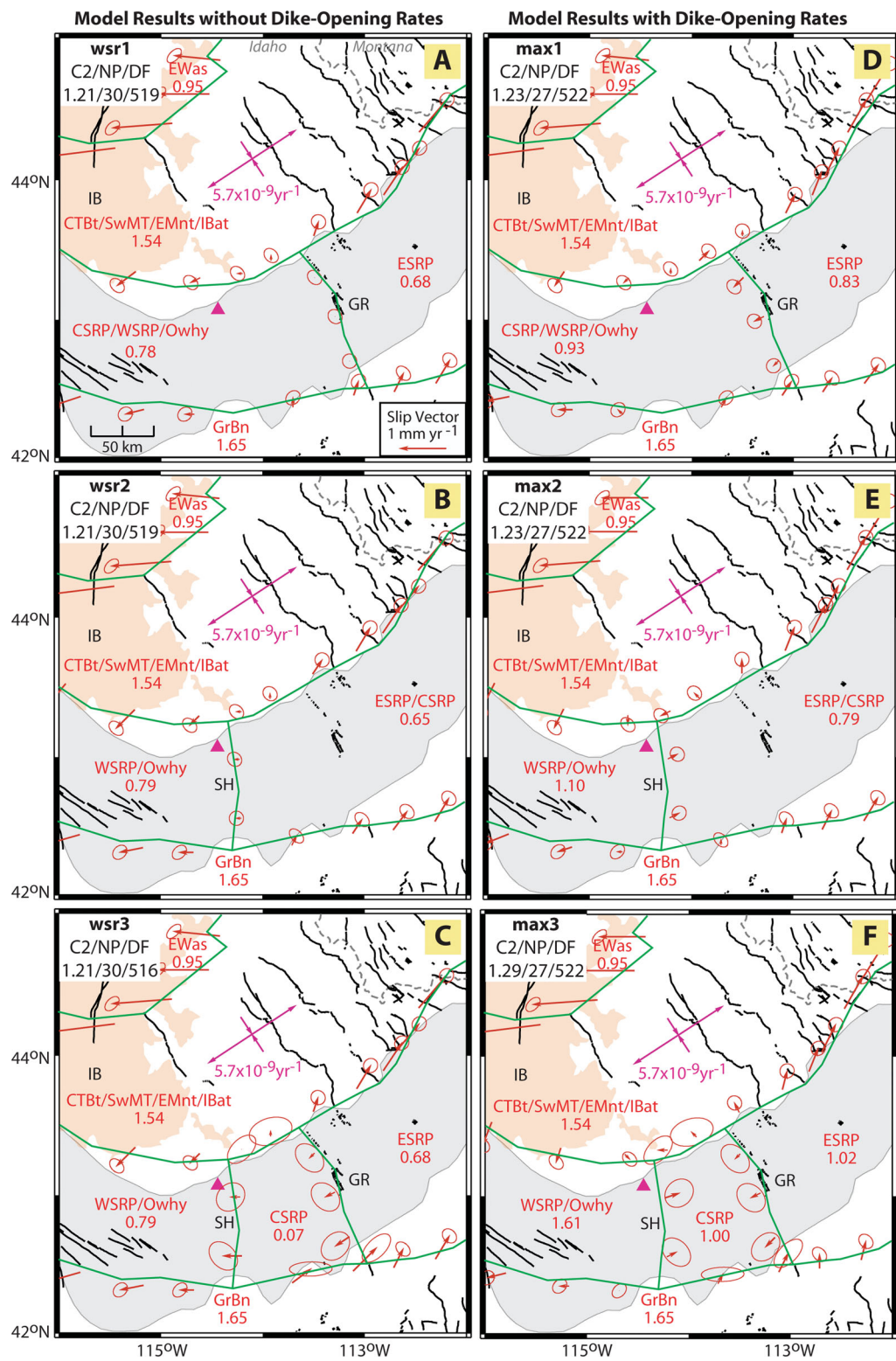


Figure 8. Maps show the slip vectors (red arrows with 70 per cent confidence ellipses) along the hangingwall of block boundaries (green lines) that represent the Great Rift (GR) and Shoshone (SH) volcanic rift zones. Models (a) wsr1, (b) wsr2 and (c) wsr3 allow slip-vector magnitudes and azimuths to vary in the inversions. Models (d) max1, (e) max2 and (f) max3 have constrained magnitudes and azimuths of the slip vectors for the dyke-opening rates estimated based on field measurements in the Great Rift (see text). The model name is given above the inversion results shown below C2/NP/DF, which corresponds to reduced chi-square (C2), number of free parameters (NP) and degrees of freedom (DF). Each block (green lines) is labelled with its name (red letters) and reduced chi-square (red number) fit of the velocities. Principal horizontal strain rates (pink arrows) are labelled with the extensional strain rate (pink letters). See Fig. 1 caption for other map contents.

Table 3. Azimuths and dyke-opening rates used in the models and predicted from the inversions.

Model	Block Fault Segment	Input Parameters			Model Predictions	
		Azimuth (°N)	Minimum Rate (mm yr ⁻¹)	Maximum Rate (mm yr ⁻¹)	Azimuth (°N)	Dyke-opening Rate (mm yr ⁻¹)
max1	Northern Great Rift	245 ± 20	0.16	2.03	233	0.29
	Central Great Rift	245 ± 20	0.16	2.03	230	0.22
	Southern Great Rift	245 ± 20	0.16	2.03	225	0.16
max2	Northern Shoshone	90 ± 20	0.16	2.03	76	0.23
	Southern Shoshone	90 ± 20	0.16	2.03	70	0.16
max3	Northern Great Rift	245 ± 20	0.16	2.03	225	0.16
	Central Great Rift	245 ± 20	0.16	2.03	232	0.23
	Southern Great Rift	245 ± 20	0.16	2.03	234	0.31
	Northern Shoshone	90 ± 20	0.16	2.03	80	0.33
	Southern Shoshone	90 ± 20	0.16	2.03	70	0.16
vrz1	Northern Great Rift	245 ± 20	0.96	1.36	226	1.02
	Central Great Rift	245 ± 20	0.96	1.36	225	0.99
	Southern Great Rift	245 ± 20	0.96	1.36	225	0.96

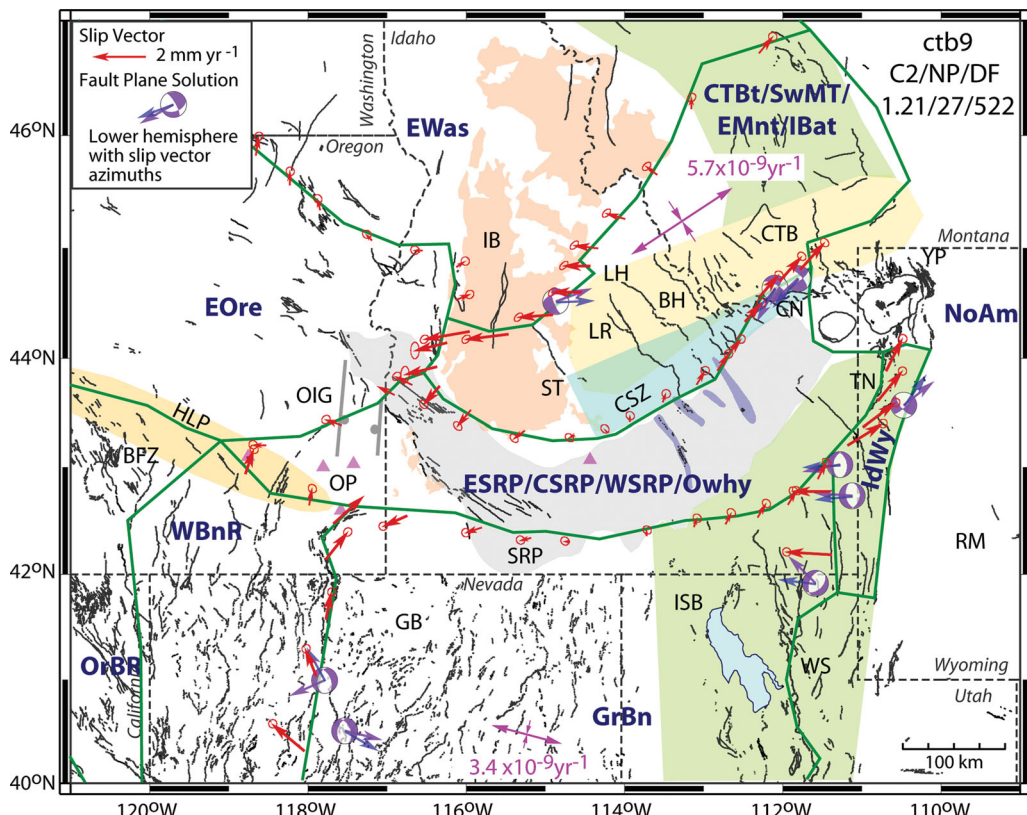


Figure 9. Map showing slip vectors along free-slipping (no fault locking) block boundaries for the preferred model ctb9. Red arrows (with 70 per cent confidence ellipses) show slip vectors for motions along boundaries (green lines) that are between two blocks with different angular velocities; their tails are on the moving block. Lower-hemisphere focal mechanisms show slip vectors (purple) compared with predicted slip vectors (blue) from the inversion (see Supporting Information). Each block is labelled in blue letters with its name or with several names (e.g. CTBt/SwMT/EMnt/IBat) to indicate the region has multiple blocks with the same pole. Principal horizontal strain rates (pink arrows) are labelled with extensional strain rates (pink letters). See Fig. 1 caption for other map contents.

estimates of what the velocities should be from the 1983 M 6.9 Borah Peak, Idaho and 1959 M 7.3 Hebgen Lake, Montana earthquakes (Fig. 1). Alternatively, we evaluate the 1994–2010 velocity field for the presence of a viscoelastic relaxation signal. First, we generate predicted velocities for the Borah Peak and Hebgen Lake earthquakes at all of our GPS sites using the Earth structure and earthquake source parameters of Nishimura & Thatcher (2003) and

the program VISCO1D (Pollitz 1992). As used by Nishimura & Thatcher (2003), the structure is a 40-km thick elastic crust overlying a mantle of viscosity 4×10^{18} Pa s. The surface velocities are estimated for June 2002, which is a representative time of our GPS measurements. In keeping with Nishimura & Thatcher (2003), we use three separate planar slip sources (one for Borah Peak and two for Hebgen Lake) and reproduce the velocity field shown in their

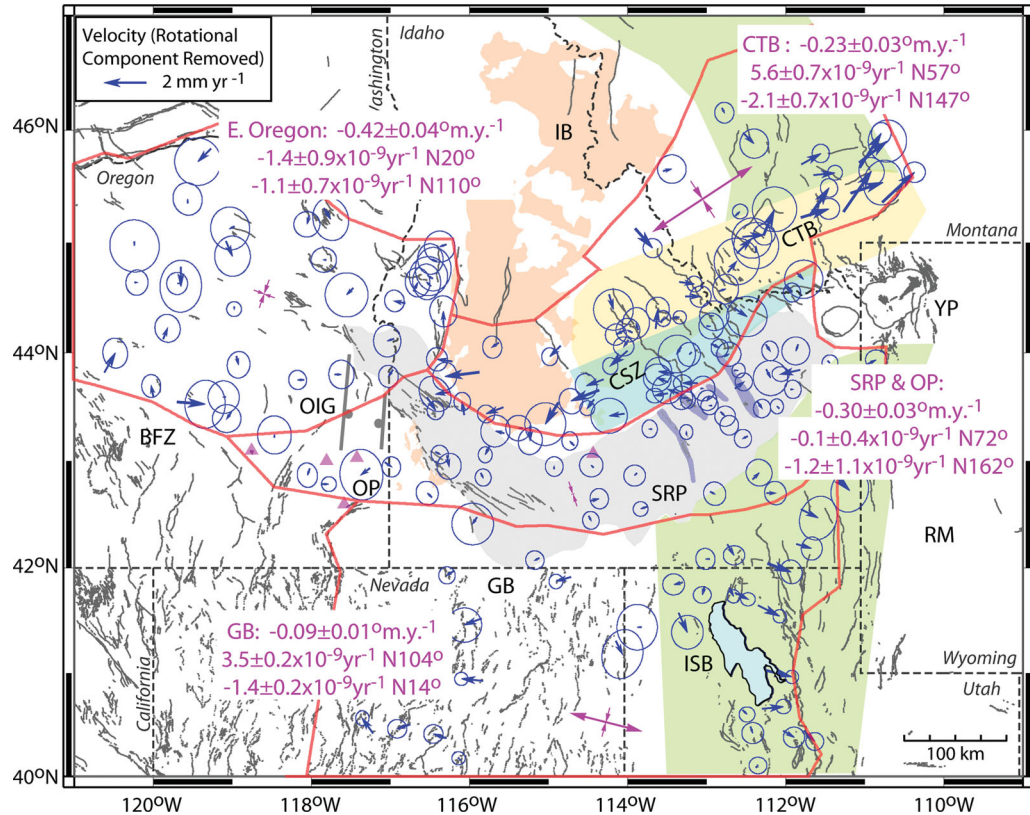


Figure 10. Velocities (blue vectors with 70 per cent confidence ellipses) show remaining gradients after subtracting out their respective rotational components. Horizontal strain rates (pink arrows) and vertical-axis rotation rates were calculated using observed velocities within the regions defined by the orange lines. Labels list tectonic province, clockwise rotation rate and strain rates for the two principal horizontal axes (pink letters). See Fig. 1 caption for other map contents.

Fig. 11 (see Supporting Information). Secondly, we run six tests to evaluate whether post-seismic signals are present in the current velocity field.

In the first test, model s1mr, we subtract the predicted viscoelastic relaxation velocities of Nishimura & Thatcher (2003) from the observed velocities at each site and run the inversion using the preferred model ctb9 to test whether a better fit results. This model has a larger $\chi^2_\eta = 1.53$, which is a >99 per cent greater misfit over $\chi^2_\eta = 1.21$ from model ctb9. In the second test, model s2mr is similar to s1mr except that we allow a strain rate to be estimated for the Snake River Plain–Owyhee Oregon Plateau (ESRP/CSRP/WSRP/Owy block). Model s2mr results in a similar $\chi^2_\eta = 1.53$ as model s1mr but still a larger misfit at >99 per cent confidence level over model ctb9 without post-seismic corrections. This produces N–S contraction at a strain rate of $-2.5 \pm 0.9 \times 10^{-9} \text{ yr}^{-1}$ in the Snake River Plain but no significant E–W extension ($0.7 \pm 0.3 \times 10^{-9} \text{ yr}^{-1}$). These model results show that the lack of observed extension in the velocities within the Snake River Plain is not due to post-seismic viscoelastic relaxation effects.

To test for possible reduced relaxation velocities (relative to the Nishimura & Thatcher predictions), we run a third test (model s3mr) where we adjust a scaling factor for each of the three earthquake viscoelastic relaxation velocity fields to allow improved fit to the observations. The initial scaling factors are the slip amplitudes during the earthquakes from Nishimura & Thatcher (2003). For the three events, Borah Peak and two Hebgen Lake subevents, the amplitudes drop to zero with a decrease in the χ^2_η to 1.21, which is similar to the χ^2_η of our preferred model ctb9 without post-seismic

relaxation. Hence, we see no indications of post-seismic signals in the 1994–2010 velocity field (see Supporting Information).

The lack of distinguishable post-seismic signals for these earthquakes in the modern velocity field may indicate a lower mantle viscosity than used in the foregoing tests. To estimate the upper bound on viscosity, we conduct three more tests where each model has a different mantle viscosity (s4mr: $4 \times 10^{17.5}$; s5mr: 4×10^{17} and s6mr: $4 \times 10^{16} \text{ Pa s}$) and the same elastic crustal thickness of 40 km. The tests indicate that viscosities of $4 \times 10^{17} \text{ Pa s}$ (s5mr) or $4 \times 10^{16} \text{ Pa s}$ (s6mr) result in lower predicted post-seismic velocities than with a viscosity of $4 \times 10^{17.5} \text{ Pa s}$ (s4mr) but still produce misfits ($\chi^2_\eta = 1.26, 1.25, 1.36$, respectively) that are larger than that for model ctb9 at over one-sigma (see Supporting Information). From these evaluations, we conclude that time-varying components due to viscoelastic relaxation from the Borah Peak and Hebgen Lake earthquakes have either ceased as of 2002 or are too small to be evident in the observed velocities.

5 DISCUSSION

We find three significant results from the velocity field: (1) the Snake River Plain appears to be moving as a nearly coherent block with uniform motion at $\sim 3 \text{ mm yr}^{-1}$ to the southwest relative to North America with slow internal deformation; (2) shear is required along the northwest and southeast boundaries of the Snake River Plain and (3) the Northern Basin and Range region is within the large-scale clockwise rotation observed over the entire Pacific Northwest.

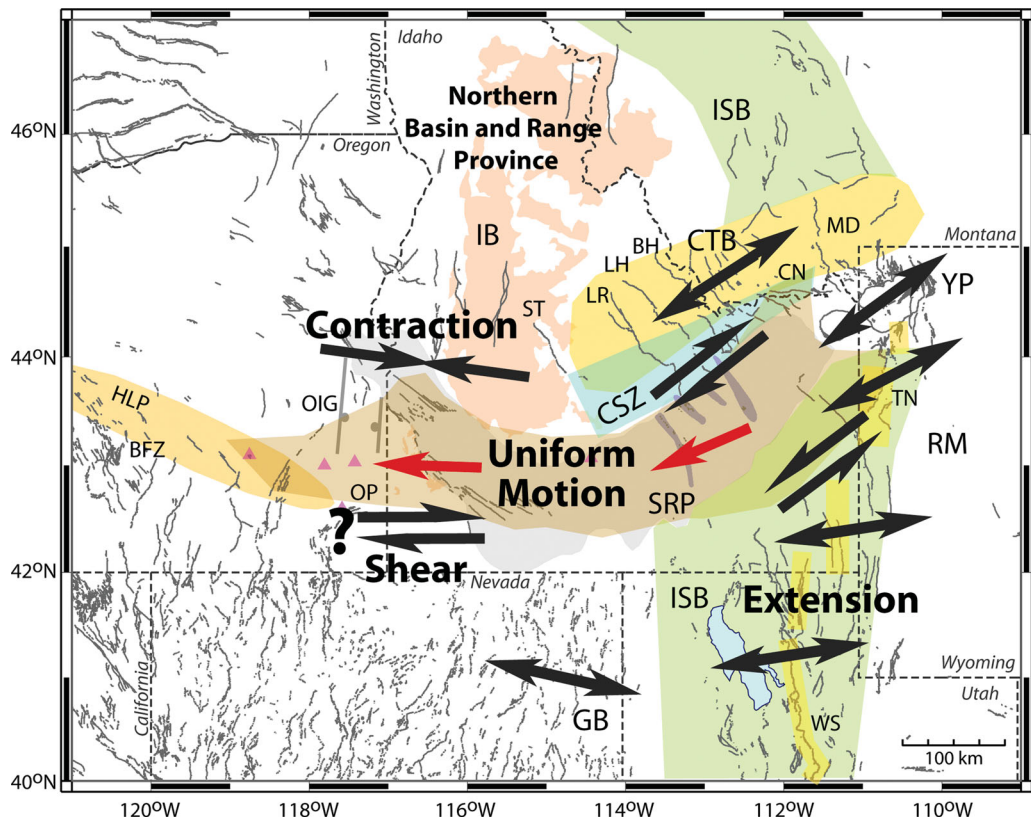


Figure 11. Interpretation of crustal deformation (black and red arrows) in the Northern Basin and Range Province based on GPS and earthquake data. The Snake River Plain has little internal deformation exhibiting coherent block-like behaviour and uniform motion (red arrows). Shear along its boundaries separates the Snake River Plain from the adjacent actively extending Intermountain Seismic Belt (thick yellow lines) and Centennial Tectonic Belt (yellow shading). See Fig. 1 for other map contents.

We explore the implications of the GPS results combined with other data and previous interpretations to develop a new regional interpretation of deformation within the Northern Basin and Range Province.

5.1 Snake river plain coherent block behaviour

Our results indicate that a sizable region (~ 125 km wide by 650 km long) has velocities with uniform magnitudes (~ 3 mm yr^{-1}) extending from the eastern to western Snake River Plain and beyond the Snake River Plain's physiographic boundaries (Fig. 10). The uniformity of velocities suggests that little internal deformation is presently occurring within the Snake River Plain and Owyhee–Oregon Plateau. The same region has much less seismicity relative to the surrounding Basin and Range regions (Fig. 6a) in the period from 1960 to 2010. Historical earthquake compilations for the Snake River Plain and Owyhee–Oregon Plateau indicate that only one earthquake of magnitude ≥ 5.5 may have occurred over the last ~ 160 yr in the region of low-strain (Oaks *et al.* 1992; Niewendorp & Neuhaus 2003; Carpenter 2010). Infrequent and small magnitude microearthquakes ($M < 2.0$) have occurred in response to tension within the eastern Snake River Plain (Jackson *et al.* 1993; Carpenter 2010). In addition, periodic basalt dyke intrusion has continued into the late Pleistocene or Holocene indicating volcanic rifting within the low-strain rate region well after (> 4 Myr) the cessation of hotspot volcanism (e.g. Hart *et al.* 1984; Kuntz *et al.* 1986; Othberg *et al.* 1995; Bondre 2006). Repose intervals (lengths of time between eruptions) of dyke-fed basalt volcanism

in the eastern Snake River Plain, western Snake River Plain and Owyhee–Oregon Plateau are estimated to be on the order of 10^4 to $> 10^6$ yr (Kuntz *et al.* 1992; Shoemaker & Hart 2002; Wood & Clemons 2002). Thus, these seismic and volcanic observations suggest the region is not entirely rigid because some internal deformation in the form of brittle fracture occurs in the Snake River Plain and Owyhee–Oregon Plateau.

Dyke intrusion may accommodate very low rates of extension within the Snake River Plain and Oregon–Owyhee Plateau as suggested by Chadwick *et al.* (2007) and Holmes *et al.* (2008). The extensive coverage of uniform velocities and low strain rate indicates that previous dyke-intrusion events are not sufficient to extend the Snake River Plain on a regional scale in the present. Models that allow dyke-opening rates of 0.16 – 0.33 mm yr^{-1} (Table 3) across the Great Rift and Shoshone volcanic rift zones do not fit the velocities (Fig. 8). While a dyke intrusion event may occur in any one volcanic rift zone, such an event will not move the entire 250 km length of the lithosphere (i.e. ESRP and CSRPs blocks combined) at one time. As explained by Payne *et al.* (2008), using an analogy with the 2005 Afar, Africa dyke event, the deformation field of a dyke intrusion event in the Snake River Plain will be localized over an area 50 km wide (Wright *et al.* 2006). At many tens of kilometres from the dyke event, the lithosphere moves steadily and is not deformed by the localized dyke-induced deformation field (e.g. LaFemina *et al.* 2005; Pederson *et al.* 2009). Hence, extension across a volcanic rift zone at ~ 2.0 mm yr^{-1} (Table 3), for example, would be clearly visible in the steady velocity field away from the volcanic rift zone. In addition, the strain rate of $1.3 \pm 2.3 \times 10^{-9}$ yr^{-1} across four volcanic rift zones (Profile B, Fig. 4) indicates

a very low rate of extension at a short wavelength (0.13 mm yr^{-1} over 100 km). Over the longer distance of 650 km, there appears to be no net extension. The higher topography of the Yellowstone Plateau to the northeast (Fig. 2) could produce a long-wavelength, compressive stress along the long axis of the Snake River Plain. Although, we do not know the magnitude of the stress, the deformation it produces would not mask shorter-wavelength ($\sim 25 \text{ km}$) GPS signals that would result from higher rates of extension within the narrow volcanic rift zones. The volcanic rift zones may be more like those near Kilauea in Hawaii, where dyke intrusion events produce local dilation of the crust with accompanying magmatic extrusion, but do not accommodate crustal extension in the far-field (i.e. the Pacific Plate is not breaking apart; e.g. Desmarais & Segall 2006). Accordingly, Snake River Plain volcanic rift zones may be a response to hotspot volcanism but may not be related to crustal extension as in the adjacent Basin and Range regions.

The very low rate of deformation within the Snake River Plain and Owyhee–Oregon Plateau could be the result of either greater lithospheric strength or lower internal differential stress. The Snake River Plain and Owyhee–Oregon Plateau could have increased strength (e.g. Anders & Sleep 1992; DeNosaquo *et al.* 2009) because this region has undergone significant crustal modifications associated with hotspot bimodal volcanism (e.g. Hill & Pakiser 1967; Sparlin *et al.* 1982; Pakiser 1989; Peng & Humphreys 1998; Stachnik *et al.* 2008; Yuan *et al.* 2010; Cox *et al.* 2011). While mafic densification of the mid- to lower-crust over most of the Snake River Plain may increase its strength, it is not sufficient to resist all tensile brittle fracture because dyke intrusion has continued into the Holocene and infrequent earthquakes have been observed in some locations. Alternatively, a low strain rate could result from low differential stresses acting upon the Snake River Plain and Owyhee–Oregon Plateau. Humphreys & Coblenz (2007) evaluated the importance of loads applied to plate boundaries and those created internally within the North American Plate due to gravitational potential energy (GPE) variations. Their best-fit models suggest that GPE-derived stress contributes to driving extensional orogenic collapse in the western U.S. and that without it, no significant extension would occur. They also showed that GPE variations contribute to deformation at Yellowstone, which has extra GPE associated with the high geoid anomaly (Smith & Braile 1994; Smith *et al.* 2009) supported by buoyancy of a deep mantle source. Within the Yellowstone geoid anomaly, GPE variations could drive gravitational collapse at a higher rate in the higher topographic-relief Basin and Range regions outboard of the Snake River Plain (Fig. 2). The Snake River Plain is a relatively flat region with high-density crustal composition and hence has lower GPE variations. Thus, block-like behaviour of the Snake River Plain and Owyhee–Oregon Plateau region is consistent with either higher strength or lower internal stresses or both.

5.2 Shear along Snake River Plain boundaries

The slowly deforming region of the Snake River Plain and Owyhee–Oregon Plateau as compared to the extending adjacent Basin and Range Provinces kinematically requires shear along their boundaries. The slip rates for shear vary along the boundaries of the Snake River Plain and Owyhee–Oregon Plateau (Fig. 9) consistent with changes in magnitudes between the velocities in the Snake River Plain and Owyhee–Oregon Plateau relative to the adjacent Basin and Range regions (Fig. 2). Using the block model approach, we model kinematic slip along boundaries representing localized discrete faults. Examining the shear in detail, Payne (2011) suggests

that right-lateral shear is distributed over the Centennial Shear Zone and may be accommodated by strike-slip motions on multiple faults parallel to or subparallel to the NE-trending, northwestern boundary of the ESRP block. Here, we give two examples of seismicity and faulting that document where strike-slip motions accommodate shear along the northwestern and southeastern boundaries of the ESRP block.

The largest slip rates are seen along the boundaries of the eastern Snake River Plain closest to the Yellowstone Plateau. Modelling results in Fig. 9 show right-lateral strike-slip rates of up to 1.4 mm yr^{-1} at the northeast end of the Centennial Shear Zone along generally E-trending normal faults that are subparallel to the northwestern boundary of the ESRP block. Mid-Pleistocene to Holocene slip along generally E-oriented normal faults to the west and along the Centennial normal fault is consistent with right-lateral shear accommodation (Bartholomew *et al.* 2002; Anastasio *et al.* 2010). Also, focal mechanisms with right-lateral strike-slip components of motion are observed within a NE-trending zone of seismicity near the Centennial fault (Stickney 1997; Fig. 9). Along the southeastern boundary of the eastern Snake River Plain, slip rates with left-lateral oblique normal or strike-slip motions are predicted between the eastern Snake River Plain and Intermountain Seismic Belt (Fig. 9). The eastern boundary of the ESRP block coincides with the Intermountain Seismic Belt (Fig. 6a), which has long been recognized as the boundary between stable North America and active Basin and Range extension (e.g. Smith & Sbar 1974; Smith & Arabasz 1991; Smith & Braile 1994). On a regional scale, left-lateral shear accommodation is indicated by the right-stepping en echelon pattern of N-oriented Quaternary normal faults that extend from the Wasatch fault to the Teton fault (Fig. 1). North of the Teton fault, there is also a 30-km zone of right-stepping normal faults that continues into the Yellowstone Plateau (Byrd *et al.* 1994). While most focal mechanisms in the Intermountain Seismic Belt indicate slip along N-trending normal faults (Fig. 1), a recent 2010 sequence of earthquakes near the Teton fault show both left-lateral (e.g. M 4.8) strike-slip and normal focal mechanisms (Fig. 9). Also, the lower strain rate within the Snake River Plain and Owyhee–Oregon Plateau block extends into the region between the eastern Snake River Plain physiographic boundary and Intermountain Seismic Belt (Fig. 10). A lower strain rate is consistent with belt IV defined by Pierce & Morgan (1992, 2009) where faults were active from 4 to 11 Ma coeval with hotspot Tertiary silicic volcanism (Rodgers *et al.* 2002) but now exhibit little to no Quaternary activity (Pierce & Morgan 1992; 2009). We suggest that left-lateral shear predicted along the eastern boundary of the ESRP block (Figs 6a and 9) could be accommodated by pre-existing right-stepping normal faults in association with extension. Similar right-stepping faults at the southern end of the Wasatch fault adjacent to the Colorado Plateau broaden westward and are separated by the E–NE-trending sinistral Pahranagat shear zone, which is kinematically required to accommodate different rates of extension (Kreemer *et al.* 2010).

5.3 Driving mechanism for clockwise rotation

Velocity gradients in the Northern Basin and Range Province (Fig. 2) show regional-scale, vertical-axis clockwise rotation similar to Oregon and southwest Washington (McCaffrey *et al.* 2007). McCaffrey *et al.* (2007) found a similar angular velocity to ours for their Oregon and Snake River Plain blocks, although they included only ten velocities in the Snake River Plain. The closely grouped locations of the poles of the Centennial Tectonic Belt, Snake River

Plain, Idaho batholith and eastern Oregon (Fig. 7a) suggest common driving mechanisms but preclude that Yellowstone hotspot volcanism (e.g. Puskas & Smith 2009) or localized extension (i.e. Centennial Tectonic Belt) drives clockwise rotation in the Northern Basin and Range Province. We propose two regional driving mechanisms. First, the large-scale rotation is consistent with right-lateral shear associated with Pacific–North America relative motion. McCaffrey *et al.* (2007), based on the similarity of velocity gradients, suggest that shear in the Walker Lane belt drives the nearly rigid blocks in southeastern Oregon (which encompass the Owyhee and E-Ore blocks in our model, Fig. 6a) northwestward. Secondly, we suggest that extension due to gravitational collapse across the Wasatch fault and the Great Basin to the south drives the Snake River Plain and Owyhee–Oregon Plateau region westward from its southwestward motion relative to the Yellowstone Plateau (Fig. 2). We think that subduction at Cascadia contributes little if any to the large-scale rotation since the Snake River Plain is ~ 1000 km from the Cascadia thrust and rapid rotation of the overriding plate at other subduction zones generally is seen only in forearc blocks close to the trench (Wallace *et al.* 2005). In eastern Oregon, McCaffrey *et al.* (2007) determined that GPS-derived clockwise rotation rates were consistent with rates from paleomagnetic data in 15–12 Ma basalts, indicating that the decadal GPS rotation reveals long-term motions. Thus, we propose that the common locations of nearby poles of rotation for the eastern Oregon block, Centennial Tectonic Belt, Idaho batholith, Snake River Plain and Owyhee–Oregon Plateau (Fig. 7b) are long-lived. Moreover, regional-scale clockwise rotation is driven by extension across the Wasatch fault due to gravitational collapse and shear in the Walker Lane belt resulting from Pacific–Northern America relative plate motion.

6 INTERPRETATION AND CONCLUSIONS

Using the 1994–2010 horizontal velocity field together with geologic, volcanic and seismic data, we interpret both the Snake River Plain and the Owyhee–Oregon Plateau to be slowly deforming and separated by shear from the rapidly extending adjacent Basin and Range regions (Fig. 11). Detailed evaluations of the observed velocities (Figs 4 and 10) show extensional strain rates to the north in the Centennial Tectonic Belt ($5.6 \pm 0.7 \times 10^{-9} \text{ yr}^{-1}$) and to the south in the Great Basin ($3.5 \pm 0.2 \times 10^{-9} \text{ yr}^{-1}$) consistent with the distribution of seismicity, normal focal mechanisms and Quaternary normal faults. Conversely, the Snake River Plain and Owyhee–Oregon Plateau has a much lower strain rate that is not discernable from zero ($-0.1 \pm 0.4 \times 10^{-9} \text{ yr}^{-1}$). Results of our inversions with dyke-opening rates indicate that extension through dyke-intrusion occurs at a much lower rate than normal faulting in adjacent regions. The low strain rate region extending over 650 km has uniform southwestward to westward motion relative to North America, showing block-like behaviour relative to the extending adjacent Basin and Range regions (Fig. 11). The very low rate of deformation could be the result of either greater lithospheric strength due to mafic densification in the mid- to lower-crust or lower GPE variations within the low-relief and high-density crustal composition of the Snake River Plain and Owyhee–Oregon Plateau or both.

As a result of strain rate differences, shear is required along the eastern Snake River Plain boundaries (Fig. 11); right-lateral shear of up to 1.4 mm yr^{-1} along the northwestern boundary and left-lateral oblique extension of up to 1.5 mm yr^{-1} along the southeastern boundary. The largest slip rates related to this shearing occur closer

to the Yellowstone Plateau where strike-slip focal mechanisms and faults with geologic observations of shear accommodation are observed (Fig. 9). In the western Snake River Plain, our models suggest right-lateral shear along the proposed southern block boundaries near the northern termination of Basin and Range extension. The southern part of the Idaho batholith is moving west and the velocity gradients within this region suggest a lower strain rate than the extensional strain rate in the Centennial Tectonic Belt to the northeast. At the western ends of the Idaho batholith and western Snake River Plain a distinct change from faster to slower velocities suggests shortening (Fig. 11).

Our results reveal clockwise rotation over the Northern Basin and Range province at a regional scale since several tectonic provinces rotate about a common location in northern Idaho: Centennial Tectonic Belt, Idaho batholith, Snake River Plain, Owyhee–Oregon Plateau and eastern Oregon. These results preclude that Yellowstone hotspot volcanism or localized extension in the Centennial Tectonic Belt drives large-scale rotation of the region. Instead, we conclude that large-scale rotation is driven by extension across the Wasatch fault due to gravitational collapse and shear in the Walker Lane belt arising from Pacific–Northern America relative plate motion. We also suggest that the decadal GPS rotation is long-lived because rotation rates in eastern Oregon are consistent with paleomagnetic data in 15–12 Ma basalts.

ACKNOWLEDGEMENTS

We thank Bill Hammond (University of Nevada at Reno) and Wayne Thatcher (U.S. Geological Survey) for their comments that greatly improved the manuscript. We also thank Jed Hodges and Rob Berg (Idaho National Laboratory) for their help with collecting campaign GPS phase data. We thank Dr. Takuya Nishimura for generously providing information. Payne appreciates the stimulating conversations with and reviews by Seth Carpenter (Idaho National Laboratory) during development of the manuscript. Figures were generated with the Generic Mapping Tool (Wessel & Smith 1998). The research was funded in part by the Idaho National Laboratory through the U.S. Department of Energy Idaho Operations Office contract DE-AC07-05ID14517 by the National Science Foundation grant EAR-0745624 to King, and by the National Earthquake Hazards Research Program (NEHRP) grant 2010-0006 to McCaffrey.

REFERENCES

- Aly, M.H., Rodgers, D.W., Thackray, G.D. & Hughes, S.S., 2009. Recent magmatotectonic activity in the Eastern Snake River Plain–Island Park region revealed by SAR Interferometry, *J. Volc. Geotherm. Res.*, **188**, 297–304.
- Anastasio, D.J., Majerowicz, C.N., Pazzaglia, F.J. & Regalla, C.A., 2010. Late Pleistocene–Holocene ruptures of the Lima Reservoir fault, SW Montana, *J. Struct. Geol.*, **32**, 1996–2008.
- Anders, M.H. & Sleep, N.H., 1992. Magmatism and extension: the thermal and mechanical effects of the Yellowstone hotspot, *J. geophys. Res.*, **97**, 15379–15393.
- Anders, M.H., Geissman, J.W., Piety, L.A. & Sullivan, J.T., 1989. Parabolic distribution of circum-easterly Snake River Plain seismicity and latest Quaternary faulting: migratory pattern and association with the Yellowstone Hotspot, *J. geophys. Res.*, **94**, 1589–1621.
- Anders, M.H., Saltzman, J. & Hemming, S.R., 2009. Neogene tephra correlations in eastern Idaho and Wyoming: implications for Yellowstone hotspot-related volcanism and tectonic activity, *Geol. Soc. Am. Bull.*, **121**, 837–856.

- Andrews, G.D.M., Branney, M.J., Bonnichsen, B. & McCurry, M., 2008. Rhyolitic ignimbrites in the Rogerson graben, southern Snake River Plain volcanic province: volcanic stratigraphy, eruption history, and basin evolution, *Bull. Volc.*, **70**, 269–291.
- Armstrong, R.L., Leeman, W.P. & Malde, H.E., 1975. Quaternary and Neogene volcanic rocks of the Snake River Plain, Idaho, *Am. J. Sci.*, **275**, 225–251.
- Bartholomew, M.J., Stickney, M.C., Wilde, E.M. & Dundas, R.G., 2002. Late Quaternary paleoseismites: syndepositional features and section restoration used to indicate paleoseismicity and stress-field orientations during faulting along the main Lima Reservoir Fault, southwestern Montana, in *Ancient Seismites*, Geol. Soc. Am. Special Paper 359, pp. 29–47, eds Ettensohn, R.F., Rast, N. & Brett, C.E., Geological Society of America, Boulder, CO.
- Bock, Y. et al., 1997. Southern California Permanent GPS Geodetic Array: continuous measurements of crustal deformation between the 1992 Landers and 1994 Northridge earthquakes, *J. geophys. Res.*, **102**, 18 013–18 033.
- Bond, J.G., Kauffman, J.D., Miller, D.A. & Venkatakrishnan, R., 1978. Geologic map of Idaho, *Idaho Bureau of Mines and Geology*, Scale 1: 500000.
- Bondre, N.R., 2006. Field and geochemical investigation of basaltic magmatism from the western United States and western India, *MSc thesis*, Miami University, Oxford, OH (unpublished).
- Bonnichsen, B., Leeman, W.P., Honjo, N., McIntosh, W.C. & Godchaux, M.M., 2008. Miocene silicic volcanism in southwestern Idaho: geochronology, geochemistry, and evolution of the central Snake River Plain, *Bull. Volc.*, **70**, 315–342.
- Byrd, J.O.D., Smith, R.B., & Geissman, J.W., 1994. The Teton fault, Wyoming: topographic signature, neotectonics, and mechanisms of deformation, *J. geophys. Res.*, **99**, 20 095–20 122.
- Carpenter, N.S., 2010. Compilation of Earthquakes from 1850–2007 within 200 miles of the Idaho National Laboratory, *Battelle Energy Alliance External Report INL /EXT-10-19120*, 65pp.
- Chadwick, J.D., Rodgers, D.W. & Payne, S.P., 2007. Contemporary tectonic motion of the eastern Snake River Plain, Idaho: a global positioning system study, 1995–2004, *Tectonics*, **26**, TC6005, doi:10.1029/2005TC001914.
- Chang, W.-L., Smith, R.B., Wicks, C., Farrell, J.M. & Puskas, C.M., 2007. Accelerated uplift and magmatic intrusion of the Yellowstone Caldera, 2004–2006, *Science*, **318**, 952–956.
- Chang, W.-L., Smith, R.B., Puskas, C.M. & Farrell, J.M., 2010. Kinematics and magmatic modeling of an extraordinary period of Yellowstone caldera uplift, 2004–2009, from GPS and InSAR observations, *Geophys. Res. Lett.*, **37**, L23302, doi:10.1029/2010GL045451.
- Christiansen, R. L., 2001. The Quaternary and Pliocene Yellowstone Plateau volcanic field of Wyoming, Idaho, and Montana, *U.S. Geol. Surv. Prof. Paper*, **729-G**, G1–G145.
- Cox, C. M., Keller, G.R. & Harder, S.H., 2011. Integrated 2-D models of crustal structure in the High Lava Plains region of eastern Oregon, *2011 EarthScope National Meeting*, 2011 May 17–20, Austin, TX.
- Cummings, M.L., Evans, J.G., Ferns, M.L. & Lees, K.R., 2000. Stratigraphic and structural evolution of the middle Miocene synvolcanic Oregon–Idaho graben, *Geol. Soc. Am. Bull.*, **112**, 668–682.
- DeNosaquo, K.R., Smith, R.B. & Lowry, A.R., 2009. Density and lithospheric strength models of the Yellowstone–Snake River Plain volcanic system from gravity and heat flow data, *J. Volc. Geotherm. Res.*, **188**, 108–127.
- Desmarais, E.K. & P. Segall, 2006. Transient deformation following the 30 January 1997 dike intrusion at Kilauea volcano, Hawai'i, *Bull. Volc.*, **69**, doi:10.1007/s00405-006-0080-7.
- Doser, D.I. & Smith, R.B., 1985. Source parameters of the 28 October 1983 Borah Peak, Idaho earthquake from body wave analysis, *Bull. seism. Soc. Am.*, **75**, 1041–1051.
- Dow, J.M., Neilan, R.E. & Rizos, C., 2009. The International GNSS Service in a changing landscape of Global Navigation Satellite Systems, *J. Geodyn.*, **83**, 191–198.
- Draper, D.S., 1991. Late Cenozoic bimodal magmatism in the northern Basin and Range province of southeastern Oregon, *J. Volc. Geotherm. Res.*, **47**, 299–328.
- Gaschnig, R.M., Vervoort, J.D., Lewis, R.S. & McClelland, W.C., 2009. Migrating magmatism in the northern US Cordillera: in situ U-Pb geochronology of the Idaho Batholith, *Contrib. Mineral Petrol.*, **159**, doi:10.1007/s00410-009-0459-5.
- Geist, D. & Richards M., 1993. Origin of the Columbia Plateau and Snake River Plain: deflection of the Yellowstone plume, *Geology*, **21**, 789–792.
- Hammond, W.C. & Thatcher, W., 2004. Contemporary tectonic deformation of the Basin and Range province, western United States: 10 years of observation with the Global Positioning System, *J. geophys. Res.*, **109**, doi:10.1029/2003JB002746.
- Hammond, W. C., Blewitt, G. & Kreemer, C., 2011. Block modeling of crustal deformation of the northern Walker Lane and Basin and Range from GPS velocities, *J. geophys. Res.*, **116**, B04402, doi:10.1029/2010JB007817.
- Hart, W.K., Aronson, J.L. & Mertzman, S.A., 1984. Areal distribution and age of low-K, high alumina olivine tholeiite magmatism in the northwestern Great Basin, *Geol. Soc. Am. Bull.*, **95**, 185–195.
- Herring, T. et al., 2008. SNARF 2.0: a regional reference frame for North America, *EOS, Trans. Am. geophys. Un.*, **89**, Jt Assem. Suppl., Abstract G21B-01.
- Herring, T.A., King, R.W. & McCluskey, S.C., 2010. *Introduction to GAMIT/GLOBK, Release 10.4*, Massachusetts Institute of Technology, Cambridge, MA. Available at: <http://www-gpsg.mit.edu/~simon/gtk/docs.htm>.
- Hill, D. P. & Pakiser, L.C., 1967. Seismic-refraction study of crustal structure between the Nevada Test Site and Boise, Idaho, *Geol. Soc. Am. Bull.*, **78**, 685–704.
- Holmes, A.A.J., Rodgers, D.W. & Hughes, S.S., 2008. Kinematic analysis of fractures in the Great Rift, Idaho: implications for subsurface dike geometry, crustal extension, and magma dynamics, *J. geophys. Res.*, **113**, B04202, doi:10.1029/2006JB004782.
- Humphreys, E.D. & Coblenz, D.D., 2007. North American dynamics and western U.S. tectonics, *Rev. Geophys.*, **45**, RG3001, doi:2005RG000181.
- Jackson, S.M., Wong, I.G., Carpenter, G.S., Anderson, D.M. & Martin, S.M., 1993. Contemporary seismicity in the eastern Snake River Plain, Idaho based on microearthquake monitoring, *Bull. seism. Soc. Am.*, **83**, 680–695.
- Jordan, B.J., Gruner, A.L., Duncan, R. & Deino, A., 2004. Geochronology of age-progressive volcanism of the Oregon High Lava Plains: implications for the plume interpretation of Yellowstone, *J. geophys. Res.*, **109**, B10202, doi:10.1029/2003JB002776.
- Kreemer, C., Blewitt, G. & Hammond, W. C., 2010. Evidence for an active shear zone in southern Nevada linking the Wasatch fault to the Eastern California shear zone, *Geology*, **38**, 475–478, doi:10.1130/G30477.1.
- Kuntz, M.A., Spiker, E.C., Rubin, M., Champion, D.E. & Lefebvre, R.H., 1986. Radiocarbon studies of latest Pleistocene and Holocene lava flows of the Snake River Plain, Idaho: data, lessons, interpretations, *Quat. Res.*, **25**, 163–176.
- Kuntz, M.A., Covington, H.R., & Schorr, L.J., 1992. An overview of basaltic volcanism of the eastern Snake River Plain, Idaho, in *Regional Geology of Eastern Idaho and Western Wyoming*, Geol. Soc. Am. Mem. Vol. 179, pp. 227–267, eds Link, P.K., Kuntz, M.A. & Platt, L.B., Geological Society of America, Boulder, CO.
- Kuntz, M.A., Anderson, S.R., Champion, D.E., Lanphere, M.A. & Grunwald, D.J., 2002. Tension cracks, eruptive fissures, dike, and faults related to late Pleistocene – Holocene basaltic volcanism and implications for the distribution of hydraulic conductivity in the eastern Snake River Plain, Idaho, in *Geology, Hydrogeology, and Environmental Remediation: Idaho National Engineering and Environmental Laboratory, Eastern Snake River Plain, Idaho*, Geol. Soc. Am. Special Paper 353, pp. 111–133, eds Link, P.K. & Mink, L.L., Geological Society of America, Boulder, CO.
- Kuntz, M.A., Skipp, B., Champion, D.E., Gans, P.B., Van Sistine, D.P. & Snyders, S.R., 2007. Geologic map of the Craters of the Moon 30' x 60' quadrangle, Idaho, U.S. Geol. Survey Sci. Investigation Map, SIM-2969, scale 1: 100,000.

- LaFemina, P.C., Dixon, T.H., Malservisi, R., Árnadóttir, T., Sturkell, E., Sigmundsson, F. & Einarsson, P., 2005. Geodetic GPS measurements in south Iceland: strain accumulation and portioning in a propagating ridge system, *J. geophys. Res.*, **110**, B11405, doi:10.1029/2005JB003675.
- Lawrence, R.D., 1976. Strike-slip faulting terminates the Basin and Range province in Oregon, *Geol. Soc. Am. Bull.*, **87**, 846–850.
- Leeman, W.P., 1982. Development of the Snake River Plain–Yellowstone Plateau Province, Idaho and Wyoming: an overview and petrologic model, in Bonnichsen, B. and Breckenridge, R.M., Cenozoic Geology of Idaho, *Idaho Geol. Surv. Bull.*, **26**, 155–178.
- Leeman, W.P., Oldow, J.S. & Hart, W.K., 1992. Lithosphere-scale thrusting in the western U.S. Cordillera as constrained by Sr and Nd isotopic transitions in Neogene volcanic rocks, *Geology*, **20**, 63–66.
- Leeman, W.P., Annen, C. & Dufek, J., 2008. Snake River Plain–Yellowstone silicic volcanism: implications for magma genesis and magma fluxes, *Geol. Soc. Lond. Spec. Publ.*, **304**, 235–259.
- Leeman, W.P., Schutt, D.L. & Hughes, S.S., 2009. Thermal structure beneath the Snake River Plain: implications for the Yellowstone hotspot, *J. Volc. Geotherm. Res.*, **188**, 57–67.
- Mabey, D.R., 1976. Interpretation of a gravity profile across the western Snake River Plain, Idaho, *Geology*, **4**, 53–55.
- Mankinen, E.A., Hildenbrand, T.G., Zientek, M.L., Box, S.E., Bookstrom, A.B., Carlson, M.H. & Larsen, J.C., 2004. Guide to geophysical data for the Northern Rocky Mountains and adjacent areas, Idaho, Montana, Washington, Oregon, and Wyoming, U.S. Geol. Surv. Open-File Report, 2004–1413.
- McCaffrey, R., 1995. DEFNODE users' guide. Available at: <http://sps.unavco.org/modeling/#defnode>.
- McCaffrey, R., 2002. Crustal block rotations and plate coupling, in Stein, S. & Freymueller, J., eds., *Plate Boundary Zones, Am. Geophys. Un. Geodyn. Ser.*, **30**, 101–122.
- McCaffrey, R., 2005. Block kinematics of the Pacific – North America plate boundary in the southwestern US from inversion of GPS, seismological, and geologic data, *J. geophys. Res.*, **110**, B07401, doi:10.1029/2004JB003307.
- McCaffrey, R., 2009. Time-dependent inversion of three-component continuous GPS for steady and transient sources in northern Cascadia, *Geophys. Res. Lett.*, **36**, L07304, doi:10.1029/2008GL036784.
- McCaffrey, R. et al., 2007. Fault locking, block rotation and crustal deformation in the Pacific Northwest, *Geophys. J. Int.*, **169**, 1315–1340.
- McCurry, M., Hayden, K.P., Morse, L.H. & Mertzman, S., 2008. Genesis of post-hotspot, At-type rhyolite of the Eastern Snake River Plain volcanic field by extreme fractional crystallization of olivine tholeiite, *Bull. Volc.*, **70**, 361–383.
- McQuarrie, N. & Rodgers, D.W., 1998. Subsidence of a volcanic basin by flexure and lower crustal flow: the eastern Snake River Plain, Idaho, *Tectonics*, **17**, 203–220, doi:10.1029/97TC03762.
- Morgan, L.A. & McIntosh, W.C., 2005. Timing and development of the Heise volcanic field, Snake River Plain, Idaho, western USA, *Bull. Geol. Soc. Am.*, **117**, 288–306.
- Niewendorp, A. & Neuhaus, M.E., 2003. Map of selected earthquakes for Oregon, 1841 through 2002, State of Oregon Department of Geology and Mineral Industries Open-file Report, 03–02.
- Nishimura, T. & Thatcher, W., 2003. Rheology of the lithosphere inferred from postseismic uplift following the 1959 Hebgen Lake earthquake, *J. geophys. Res.*, **108**, 2389, doi:10.1029/2002JB002191.
- Oaks, S.D., Jackson, S.M., & Wong, I.G., 1992. An investigation of the 11 November 1905 Shoshone, Idaho earthquake: implications for seismic hazards within the eastern Snake River Plain, *Seism. Res. Lett.*, **63**, 22.
- Othberg, K.L., Bonnichsen, B., Swisher III, C.C. & Godchaux, M.M., 1995. Geochronology and geochemistry of Pleistocene basalts of the western Snake River Plain and Smith Prairie, Idaho, *Isochron. West.*, **62**, 16–29.
- Pakiser, L.C., 1989. Geophysics of the Intermontane system, in *Geophysical Framework of the Continental United States*, Geol. Soc. Am. Mem. Vol. 172 pp. 235–247, eds Pakiser, L.C. & Mooney, W.D., Geological Society of America, Boulder, CO.
- Parsons, T., Thompson, G.A. & Smith, R.P., 1998. More than one way to stretch: a tectonic model for extension along the track of the Yellowstone hotspot and adjacent Basin and Range Province, *Tectonics*, **17**, 221–234.
- Payne, S.J., 2011. Kinematics of the Snake River Plain and Centennial Shear Zone, Idaho, from GPS and earthquake data, *PhD thesis*, University of Idaho, Moscow, ID (unpublished).
- Payne, S.J., McCaffrey, R. & King, R.W., 2008. Strain rates and contemporary deformation in the Snake River Plain and surrounding Basin and Range from GPS and seismicity, *Geology*, **36**, 647–650.
- Payne, S.J., McCaffrey, R. & King, R.W., 2009. Time-dependent inversion of three-component continuous GPS for steady and transient effects of the Yellowstone Hotspot on the Snake River Plain, Idaho, *EOS, Trans. Am. Geophys. Un.*, **90** (52), Fall Meet. Suppl. G33A-0622.
- Pederson, R., Sigmundsson, F. & Masterlark, T., 2009. Rheologic controls on inter-rifting deformation of the Northern Volcanic zone, Iceland, *Earth planet. Sci. Lett.*, **281**, 14–26.
- Peng, X. & Humphreys, E.D., 1998. Crustal velocity structure across the eastern Snake River Plain and the Yellowstone swell, *J. geophys. Res.*, **103**, 7171–7186.
- Pennington, W.D., Smith, R.B. & Tremble, A.B., 1974. A microearthquake study of parts of the Snake River Plain and central Idaho, *Bull. seism. Soc. Am.*, **64**, 307–312.
- Pierce, K.L. & Morgan, L.A., 1992. The track of the Yellowstone hotspot: volcanism, faulting, and uplift; in *Regional Geology of Eastern Idaho and Western Wyoming*, Geol. Soc. Am. Mem. Vol. 179, pp. 1–53, eds Link, P.K., Kuntz, M.A., & Platt, L.B., Geological Society of America, Boulder, CO.
- Pierce, K.L. & Morgan, L.A., 2009. Is the track of the Yellowstone hotspot driven by a deep mantle plume? – Review of volcanism, faulting, and uplift in light of new data, *J. Volc. Geotherm. Res.*, **188**, 1–25.
- Pollitz, F.F., 1992. Postseismic relaxation theory on the spherical Earth, *Bull. seism. Soc. Am.*, **82**, 422–453.
- Press, W.H., Flannery, B.P., Teukolsky, S.A. & Vetterling, W.T., 1989. *Numerical Recipes*, Cambridge University Press, Cambridge.
- Puskas, C.M. & Smith, R.B., 2009. Intraplate deformation and microplate tectonics of the Yellowstone Hotspot and surrounding western U.S. interior, *J. geophys. Res.*, **114**, B04410, doi:10.1029/2008JB005940.
- Puskas, C.M., Smith, R.B., Meertens, C.M. & Chang, W.-L., 2007. Crustal deformation of the Yellowstone–Snake River Plain volcano-tectonic system: campaign and continuous GPS observations, 1987–2004, *J. geophys. Res.*, **112**, B03401, doi:10.1029/2006JB004325.
- Richins, W.D., Pechmann, J.C., Smith, R.B., Langer, C.J., Goter, S.K., Zollweg, J.E. & King, J.J., 1987. The 1983 Borah Peak, Idaho earthquake and its aftershocks, *Bull. seism. Soc. Am.*, **77**, 694–723.
- Rodgers, D.W., Hackett, W.R. & Ore, H.T., 1990. Extension of the Yellowstone Plateau, eastern Snake River Plain, and Owyhee plateau, *Geology*, **18**, 1138–1141.
- Rodgers, D.W., Ore, H.T., Bobo, R.T., McQuarrie, N. & Zentner, N., 2002. Extension and subsidence of the eastern Snake River Plain, Idaho, in *Tectonic and magmatic evolution of the Snake River Plain Volcanic Province*, Idaho Geological Survey Vol. 30, pp. 121–155, eds Bonnichsen, B., White, C.M. & McCurry, M., Idaho Geological Survey, Moscow, ID.
- Saltzer, R.L. & Humphreys, E.D., 1997. Upper mantle P wave velocity structure of the eastern Snake River Plain and its relationship to geodynamic models of the region, *J. geophys. Res.*, **102**, 11829–11841.
- Savage, J.C., Gan, W. & Svart, J.L., 2001. Strain accumulation and rotation in the eastern California shear zone, *J. geophys. Res.*, **106**, 21995–22007.
- Shervais, J.W. & Hanan, B.B., 2008. Lithospheric topography, tilted plumes, and the track of the Snake River–Yellowstone Hotspot, *Tectonics*, **27**, TC5004, doi:10.1029/2007TC002181.
- Shervais, J.W., Shroff, G., Vetter, S.K., Matthews, S., Hanan, B.B. & McGee, J.J., 2002. Origin and evolution of the western Snake River Plain: implications from stratigraphy, faulting, and the geochemistry of basalts near Mountain Home, Idaho, in *Tectonic and Magmatic Evolution of the Snake River Plain Volcanic Province*, Idaho Geological Survey Vol. 30, pp. 343–361, eds Bonnichsen, B., White, C.M. & McCurry, M., Idaho Geological Survey, Moscow, ID.

- Shervais, J.W., Vetter, S.K. & Hanan, B.B., 2006. Layered mafic sill complex beneath the eastern Snake River Plain: evidence from cyclic geochemical variations in basalt, *Geology*, **34**, 365–368.
- Shoemaker, K.A. & Hart, W.K., 2002. Temporal controls on basalt genesis and evolution on the Owyhee Plateau, Idaho and Oregon, in *Tectonic and Magmatic Evolution of the Snake River Plain Volcanic Province*, Idaho Geological Survey Vol. 30, pp. 313–328, eds Bonnichsen, B., White, C.W. & McCurry, M., Idaho Geological Survey, Moscow, ID.
- Siebert, L. & Simkin, T., 2002. Volcanoes of the World: an illustrated catalog of Holocene volcanoes and their eruptions. *Smithsonian Institution Global Volcanism Program Digital Information Series GVP-3*, Available at: <http://www.volcano.si.edu/world/> (last accessed 2010 December 2).
- Smith, R.B. & Arabasz, W.J., 1991. Seismicity of the Intermountain Seismic Belt, in *Neotectonics of North America*, pp. 185–221, eds Slemmons, D.B., Engdahl, E.R., Zoback, M.D., & Blackwell, D.D., Geological Society of America, Boulder, CO.
- Smith, R.B. & Braile, L.W., 1994. The Yellowstone hotspot, *J. Volc. Geotherm. Res.*, **61**, 121–187.
- Smith, R.B. & Sbar, M.L., 1974. Contemporary tectonics and seismicity of the western United States with emphasis on the Intermountain Seismic Belt, *Geol. Soc. Am. Bull.*, **85**, 1205–1218.
- Smith, R.B. et al., 2009. Geodynamics of the Yellowstone hotspot and mantle plume: seismic and GPS imaging, kinematics, mantle flow, *J. Volc. Geotherm. Res.*, **188**, 26–65.
- Sparlin, M.A., Braile, L.W. & Smith, R.B., 1982. Crustal Structure of the Eastern Snake River Plain Determined from Ray Trace Modeling of Seismic Refraction Data, *J. geophys. Res.*, **87**, 2619–2633.
- Stachnik, J.C., Dueker, K., Schutt, D.L. & Yuan, J., 2008. Imaging Yellowstone plume-lithosphere interactions from inversion of ballistic and diffusive Rayleigh wave dispersion and crustal thickness data, *Geochem. Geophys. Geosyst.*, **9**, 1–21.
- Stein, S. & Gordon, R.G., 1984. Statistical tests of additional plate boundaries from plate motion inversions, *Earth planet. Sci. Lett.*, **69**, 401–412.
- Stickney, M.C., 1997. Seismic source zones in southwestern Montana, Montana Bureau of Mines and Geology Open-File Report, **366**, 52 p.
- Stickney, M.C. & Bartholomew, M.J., 1987. Seismicity and late Quaternary faulting of the northern basin and range province, Montana and Idaho, *Bull. seism. Soc. Am.*, **77**, 1602–1625.
- Stoeser, D.B., Green, G.N., Morath, L.C., Heran, W.D., Wilson, A.B., Moore, D.W. & Van Gosen, B.S., 2005. Preliminary integrated geologic map database for the United States Central States: Montana, Wyoming, Colorado, New Mexico, Kansas, Oklahoma, Texas, Missouri, Arkansas, and Louisiana, – The State of Montana, U.S. Geol. Surv. Open-file Report, 2005–1351.
- Vetter, S.K. & Shervais, J.W., 1992. Continental basalts of the Boise River Group near Smith Prairie, Idaho, *J. geophys. Res.*, **97**, 9043–9061, doi:10.1029/92JB00209.
- Walker, G.W., 1969. Geology of the High Lava Plains province, in *Mineral and Water Resources of Oregon*, pp. 77–79, Vol. 64, ed. Weissenborn, A.E., Oregon Department of Geology and Mineral Industries, Portland, OR.
- Wallace, L.M., McCaffrey, R., Beavan, J., & Ellis, S., 2005. Rapid microplate rotations and back-arc rifting at the transition between collision and subduction, *Geology*, **33**, 857–860.
- Wernicke, B.P., Christiansen, R.L., England, P.C. & Sonder, L.J., 1987. Tectonomagmatic evolution of Cenozoic extension in the North American Cordillera, *Geol. Soc. Lond. Spec. Publ.*, **28**, 223–246, doi:10.1144/GSL.SP.1987.028.01.16.
- Wessel, P. & Smith, W.H.F., 1998. New, improved version of the Generic Mapping Tools Released, *EOS, Trans. Am. geophys. Un.*, **79**, 579, doi:10.1029/98EO00426.
- Wicks, C.W., Thatcher, W., Dzurisin, F. & Svanc, J., 2006. Uplift, thermal unrest and magma intrusion at Yellowstone caldera, *Nature*, **440**, doi:10.1038/nature04507.
- Wood S.H., & Clemens, T., 2002. Geologic and tectonic history of the Western Snake River Plain, in *Tectonic and magmatic evolution of the Snake River Plain volcanic province, Idaho*, pp. 69–103, Vol. 30, eds Bonnichsen, B., White, C.M. & McCurry, M., Idaho Geological Survey Bulletin.
- Wright, T.J., Ebinger, C., Biggs, J., Ayele, A., Yirgu, G., Kier, D. & Stork, A., 2006. Magma-maintained rift segmentation at continental rupture in the 2005 Afar dyking episode, *Nature*, **442**, 291–294.
- Yuan, H., Dueker, K. & Stachnik, J., 2010. Crustal structure and thickness along the Yellowstone hotspot track: evidence for lower crustal outflow from beneath the eastern Snake River Plain, *Geochem. Geophys. Geosyst.*, **11**, Q03009 doi:10.1029/2009GC002787.

SUPPORTING INFORMATION

Additional Supporting Information may be found in the online version of this article:

Table S1. Horizontal GPS velocities used to calculate strain rates for Profiles A, B, C and D in Fig. 4.

Table S2. Horizontal GPS velocities and sigmas used to calculate weighted average velocities and errors along Profiles E, F, G and H (Fig.5).

Table S3. Slip vectors of earthquakes used in the inversions and predicted slip vector from preferred model ctb9.

Table S4. Results of F distribution tests for model pairs.

Table S5. Dyke-opening rates calculated for the Great Rift volcanic rift zone.

Table S6. Input parameters to VISCO1D from Nishimura & Thatcher (2003) for earthquake sources.

Table S7. Input parameters to VISCO1D from Nishimura & Thatcher (2003) for the earth model.

Table S8. Results of F distribution tests between post-seismic and preferred model pairs.

Table S9. Horizontal GPS velocities in the Stable North American Reference Frame (SNARF).

Figure S1. Map shows locations of focal mechanisms with slip vectors and identification numbers that correspond to Table S3.

Figure S2. Map showing the block model (green lines) and horizontal GPS velocities (red vectors with 70 per cent confidence ellipses).

Figure S3. Inversion results for models nb11 and nb13.

Figure S4. Inversion results for models nb16 and nbr3.

Figure S5. Inversion results for models ctb9 and ctb7.

Figure S6. Inversion results for models wsr1 and max1.

Figure S7. Inversion results for models wsr2 and max2.

Figure S8. Inversion results for models wsr3 and max3.

Figure S9. Inversion results for models vrz1 and esa9.

Figure S10. Inversion results for model eas9 showing GPS sites with elastic strain accumulation.

Figure S11. Plot shows reproduction of synthetic post-seismic velocities from VISCO1D generated using input parameters (e.g. mantle viscosity of $4 \times 10^{17.5}$ Pa s) from Nishimura & Thatcher (2003).

Figure S12. Plot shows synthetic post-seismic velocities at GPS sites generated using VISCO1D and input parameters (e.g. mantle viscosity of 4×10^{18} Pa s) from Nishimura & Thatcher (2003), which were used to correct the 1994–2010 velocity field for models s1mr, s2mr and s3mr.

Figure S13. Inversion results for models s1mr and s2mr.

Figure S14. Inversion results for models s3mr and s4mr.

Figure S15. Plot shows synthetic post-seismic velocities at GPS sites generated using the mantle viscosity of $4 \times 10^{17.5}$ Pa s, which were used to correct the 1994–2010 velocity field for model s4mr.

Figure S16. Plot shows synthetic post-seismic velocities at GPS sites generated using the mantle viscosity of 4×10^{17} Pa s, which were used to correct the 1994–2010 velocity field for model s5mr.
Figure S17. Plot shows synthetic post-seismic velocities at GPS sites generated using the mantle viscosity of 4×10^{16} Pa s, which were used to correct the 1994–2010 velocity field for model s6mr.

Figure S18. Inversion results for models s5mr and s6mr.

Please note: Wiley-Blackwell are not responsible for the content or functionality of any supporting materials supplied by the authors. Any queries (other than missing material) should be directed to the corresponding author for the article.